Hybrid operational modal analysis of an operative two-bladed offshore wind turbine

ter Meulen, Daan Willem Berend; Cabboi, Alessandro; Antonini, Alessandro

DOI
10.1016/j.ymssp.2024.111822

Publication date
2024

Document Version
Final published version

Published in
Mechanical Systems and Signal Processing

Mechanical Systems and Signal Processing 223 (2025) 111822

Contents lists available at ScienceDirect

Mechanical Systems and Signal Processing

journal homepage: www.elsevier.com/locate/ymssp

Hybrid operational modal analysis of an operative two-bladed offshore wind turbine

Daan Willem Berend ter Meulen [a,*], Alessandro Cabboi [b], Alessandro Antonini [a]

[a] Department of Hydraulic Engineering, Faculty of Civil Engineering and Geosciences, Delft University of Technology, Stevinweg 1, 2628CN Delft, Netherlands

[b] Department of Engineering Structures, Faculty of Civil Engineering and Geosciences, Delft University of Technology, Stevinweg 1, 2628CN Delft, Netherlands

ARTICLE INFO

Communicated by E.P.B. Reynders

Keywords:
Modal properties
Frequency domain decomposition
Power spectral density transmissibility
Kurtosis value

ABSTRACT

As with any strategic structure, vibration-based structural health monitoring techniques are often used to ensure the structurally safe operation of offshore wind turbines. Among such techniques, Operational Modal Analysis (OMA) methods allow the identification of modal properties, such as natural frequencies, mode shapes and damping, which variation might be caused by damage or operational/environmental factors. This paper investigates the application of OMA techniques on a two-bladed offshore wind turbine, which poses multiple challenges: fundamental OMA assumptions about the applied loads are violated by environmental and operational loads; the closely spaced modes of an offshore wind turbine are hard to identify; and an operative two-bladed offshore wind turbine is a time-variant system. Within this study, three OMA procedures to overcome some of the preceding challenges are discussed: (1) a standard frequency domain decomposition method; (2) a proposed enhanced transmissibility-based approach with a post-processing technique based on the Kurtosis index; and (3) a proposed refined hybrid OMA procedure that combines a transmissibility-based approach, the dedicated post-processing technique based on the Kurtosis index, and the frequency domain decomposition method. A numerical model representative of an operative two-bladed offshore wind turbine is used to compare the three procedures. Based on the comparison, the hybrid method is proven to be a promising new OMA-based procedure that outperforms the stand-alone transmissibility-based approach and the frequency domain decomposition method in identifying the modal properties of a two-bladed offshore wind turbine.

1. Introduction

In recent years, two-bladed Offshore Wind Turbines (OWTs) regained interest in finding the most profitable way of generating wind energy due to similar efficiency but much lower costs than three-bladed OWTs [1]. It goes without saying that wind industry companies want to ensure the safe operation of two-bladed OWTs by utilizing Structural Health Monitoring (SHM) strategies [2]. Any SHM strategy is essentially an inverse problem, in which, based on the measured response of the investigated structure, one may wish to infer back its current state and structural integrity. SHM strategies usually rely on state and system identification techniques. Amongst these, a branch is specifically constituted by dynamic identification algorithms. The latter aims to identify the structure's modal properties, such as natural frequencies, damping ratios, and mode shapes [3]. Within the context of linear theory, the modal

* Corresponding author.
E-mail addresses: D.W.B.terMeulen@tudelft.nl (D.W.B. ter Meulen), A.Cabboi@tudelft.nl (A. Cabboi), A.Antonini@tudelft.nl (A. Antonini).

https://doi.org/10.1016/j.ymssp.2024.111822
Received 13 September 2023; Received in revised form 28 May 2024; Accepted 8 August 2024
Available online 24 August 2024

properties form the *dynamic fingerprint* of a structure since they are intrinsically dependent on the mass, stiffness, and damping properties. However, such modal properties are not exactly constant features but are highly sensitive to environmental conditions and degradation, as observed throughout many dynamic monitoring campaigns for wind turbines discussed in the literature [4–8]. Many strategies have been proposed to tackle the time-variance of the modal properties for SHM purposes based on first tracking the modal properties over time [3,9–14] and subsequently identifying patterns in the identified data aimed at spotting anomalies that can potentially indicate damage [15–19]. Among the different methods to identify modal properties, Operational Modal Analysis (OMA) techniques only rely on post-processing the dynamic response of a structure, and no measurement of the loading force is needed [3]. Therefore, OMA approaches are rather suitable for the modal identification of wind turbine structures.

Concerning an operative two-bladed OWT, the most common OMA-based techniques are pushed to their limits in identifying the modal properties over time due to their inherent assumptions. A first limiting assumption for common OMA techniques concerns the applied loads, which are assumed to be uncorrelated and characterized by smooth and broadband spectra acting over the entire structure [3]. The nature of environmental (i.e. aerodynamic and hydrodynamic loads) and operational (i.e. rotating blades) loads acting on an operative two-bladed OWT clearly violates the loading assumptions, limiting the applicability of OMA [20]. A further challenge consists of correctly identifying the closely spaced modes of an OWT [3]. On top of that, in contrast to three-bladed OWTs, the modal properties of the tower and the support structure of a two-bladed OWT change depending on the azimuthal angle of the blades [21,22]. Hence, an operative two-bladed OWT becomes a time-variant system resulting in varying modal properties, challenging the linear time-invariant assumption of most OMA-based techniques [3].

Transmissibility-based OMA (TOMA) [23] can be used to tackle some of the prior limitations concerning the dynamic identification of an operative two-bladed OWT. The TOMA method does not depend on the nature of the applied loads and can correctly identify the modal properties for non-white noise excitations [24]. Over the last decade, multiple TOMA approaches have been proposed, generally divided into two types: the classic formulation of Response Transmissibility (RT) and the Power Spectral Density Transmissibility (PSDT) [24]. To also tackle the identification of closely spaced modes, TOMA algorithms can be applied in combination with other signal processing techniques, such as the Blind Source Separation (BSS) method [25]. To extend the dynamic identification capability of the TOMA techniques in the presence of harmonic loads, Do et al. [26] proposed a post-processing step based on a Kurtosis assessment. Furthermore, to deal with non-fully loaded structures, Araújo et al. [27] developed an enhanced PSDT procedure using a modified PSDT matrix.

This paper proposes and analyses two transmissibility-based procedures: an enhanced TOMA approach and a refined hybrid OMA procedure. The enhanced TOMA approach incorporates the findings of both Do et al. [26] and Araújo et al. [27] in the PSDT & BSS method [25]. In this way, a first promising procedure is proposed that may overcome some of the encountered limitations of the PSDT & BSS method [25]. This proposed procedure is further mentioned as *the enhanced PSDT & BSS method*. The second transmissibility-based approach is a refined hybrid OMA procedure that combines the enhanced PSDT procedure [27], the Kurtosis assessment [26], and the frequently used Frequency Domain Decomposition (FDD) method [28]. This final hybrid OMA procedure has the potential to tackle some of the mentioned challenges concerning the dynamic identification of an operative two-bladed OWT by combining the advantages of different OMA techniques. This approach is mentioned as *the hybrid OMA method* throughout the manuscript.

The performance of the two transmissibility-based procedures to identify modal properties from simulated dynamic responses is benchmarked. A representative numerical model of an operative two-bladed OWT is developed to generate different dynamic responses. Different loading scenarios are considered, such as a standstill OWT loaded by a coloured noise excitation, a standstill OWT excited by environmental loads coupled with additional background noise, and an operative OWT excited by environmental and operational loads coupled with additional background noise. Modal properties identified by the transmissibility-based procedures are compared with the known modelled modal properties. A comparison is then made between the suitability of the transmissibility-based methods and the generally used FDD [28] method. This comparison proves that the hybrid OMA method outperforms the enhanced PSDT & BSS method and the FDD method in identifying the modal properties of a two-bladed OWT. Besides assessing the performance, this study also highlights the relevance of taking advantage of different dynamic identification techniques and combining them into a sequential procedure able to overcome challenges that a single technique cannot tackle.

The structure of the document is as follows. The FDD method is revisited, and the enhanced PSDT & BSS method and the hybrid OMA method are proposed in Section 2. Section 3 describes the numerical model of an operative two-bladed OWT. Section 4 presents the modal identification results of the FDD method, the enhanced PSDT & BSS method, and the hybrid OMA method. Finally, Section 5 discusses the advantages and limitations of the hybrid OMA method.

2. Overview of OMA techniques

2.1. Benchmark criteria OMA techniques

The FDD, enhanced PSDT & BSS, and hybrid OMA methods are analysed for their effectiveness in overcoming the challenges indicated in Section 1 concerning the dynamic identification of two-bladed OWTs. Possibilities and limitations of the three different OMA approaches in addressing the challenges are reviewed based on the following three benchmark criteria applicable to both standstill and operative two-bladed OWTs:

1. Estimation of the natural frequencies, in particular of the closely spaced modes;
2. Estimation of the mode shapes, in particular of the closely spaced modes;
3. Independence of the type of excitation (e.g., environmental or operational excitation).

2.2. Frequency domain decomposition

The FDD method can be considered one of the most commonly used OMA techniques since it is user-friendly, rather intuitive and capable of identifying closely spaced modes (see benchmark criteria (1) and (2) in Section 2.1). As extensively illustrated in [28], the FDD method relies on the relationship in the frequency domain between the measured dynamic responses $\mathbf{x}(t)$ and the applied loads $\mathbf{p}(t)$, which is defined as

$$\mathbf{S}_{xx}(\omega) = \mathbf{H}(\omega)\mathbf{S}_{pp}(\omega)\mathbf{H}(\omega)^{*T} \tag{1}$$

where $\mathbf{S}_{xx}(\omega)$ and $\mathbf{S}_{pp}(\omega)$ are the auto/cross — Power Spectral Density (PSD) matrices of the dynamic responses and the applied loads, $\mathbf{H}(\omega)$ is the frequency response function of the system, and $*T$ is the conjugate transpose. The FDD method assumes that the applied loads form an uncorrelated white noise excitation acting over the entire structure. By this assumption, the $\mathbf{S}_{pp}(\omega)$ becomes a constant diagonal matrix ($\mathbf{C}$), and $\mathbf{S}_{xx}(\omega)$ can be expressed as

$$\mathbf{S}_{xx}(\omega) = \mathbf{H}(\omega)\mathbf{C}\mathbf{H}(\omega)^{*T} \propto \mathbf{H}(\omega)\mathbf{H}(\omega)^{*T}. \tag{2}$$

For a linear lightly damped system with orthogonal modes, the matrix decomposition shown in Eq. (2) can be achieved through a Singular Value Decomposition (SVD) given by

$$\mathbf{S}_{xx}(\omega) \propto \mathbf{H}(\omega)\mathbf{H}(\omega)^{*T} = \mathbf{U}(\omega)\mathbf{\Sigma}(\omega)\mathbf{V}(\omega)^{*T} = \mathbf{U}(\omega)\mathbf{\Sigma}(\omega)\mathbf{U}(\omega)^{*T} \tag{3}$$

where $\mathbf{U}(\omega)$ and $\mathbf{V}(\omega)$ are the left and right singular vector matrices, and $\mathbf{\Sigma}(\omega)$ is the singular value matrix. Note that the left and right singular vector matrices of $\mathbf{S}_{xx}(\omega)$ are similar in Eq. (3). Besides the singular value decomposition, the superposition principle characterizing linear theory provides another way of expressing $\mathbf{S}_{xx}(\omega)$ through modal coordinates defined by

$$\mathbf{S}_{xx}(\omega) = \mathbf{\Phi}\mathbf{S}_{zz}(\omega)\mathbf{\Phi}^{*T} \tag{4}$$

where $\mathbf{\Phi}$ is the structure's mode shapes matrix and $\mathbf{S}_{zz}(\omega)$ is the auto/cross — PSD matrix of the modal coordinates.

In a linear theory framework, the left singular vectors of Eq. (3) and the mode shapes of Eq. (4) are related to each other. Therefore, the modal properties of a structure are identified by applying the SVD to the PSD matrices of the dynamic responses using the following procedure:

1. Estimate the auto/cross — PSDs ($\mathbf{S}_{xx}(\omega)$) of the dynamic response;
2. Decompose $\mathbf{S}_{xx}(\omega)$ in singular values and vectors using the SVD;
3. Identify natural frequencies from peaks of the first singular values;
4. Identify mode shapes from the left singular vectors corresponding to identified singular values of step 3.

2.3. Enhanced PSDT & BSS method

The applicability to OWTs of the FDD method is limited due to the assumption that the applied loads form an uncorrelated white noise excitation acting over the entire structure. The environmental and operational loads acting on the OWT violate these loading assumptions [20], and alternative OMA methods are required that are not affected by the type of applied excitation (see benchmark criteria (3) in Section 2.1). This section proposes the enhanced PSDT & BSS method that may overcome these challenges since this transmissibility-based approach makes no assumptions about the nature of the applied loads and can even identify the closely spaced modes of an OWT (see benchmark criteria (1) and (2) in Section 2.1).

2.3.1. Power spectral density transmissibility

A transmissibility function is the ratio of two dynamic responses, $x_i(t)$ and $x_j(t)$, in the frequency domain. The PSDT is, accordingly, the ratio of the cross — PSDs of responses $x_i(t)$ and $x_j(t)$ with respect to a reference response $x_z(t)$ and estimated by

$$T_{ij}^{z}(\omega) = \frac{S_{x_i x_z}(\omega)}{S_{x_j x_z}(\omega)} \tag{5}$$

where $S_{x_i x_z}(\omega)$ is the cross — PSD of $x_i(t)$ and $x_z(t)$. It is established [29,30] that the PSDT of Eq. (5) at natural frequencies (ω_l) eliminates the forcing terms and converges to a ratio of the vibration mode's amplitudes (e.g., ϕ_{il} and ϕ_{jl}):

$$\lim_{\omega\to\omega_l} T_{ij}^{z}(\omega) = \lim_{\omega\to\omega_l} \frac{S_{x_i x_z}(\omega)}{S_{x_j x_z}(\omega)} = \frac{\phi_{il}}{\phi_{jl}} \tag{6}$$

As a result, the PSDT is (at natural frequencies) independent of the applied excitations and the selected reference response $x_z(t)$.

Araújo and Laier [30] proposed to collect the PSDTs of dynamic responses measured at L locations in a so-called PSDT matrix given by

$$\left[\mathbf{T}_j(\omega)\right] = \begin{bmatrix} S_{x_1x_1}/S_{x_jx_1} & S_{x_1x_2}/S_{x_jx_2} & \cdots & S_{x_1x_L}/S_{x_jx_L} \\ S_{x_2x_1}/S_{x_jx_1} & S_{x_2x_2}/S_{x_jx_2} & \cdots & S_{x_2x_L}/S_{x_jx_L} \\ \vdots & \vdots & \ddots & \vdots \\ S_{x_Lx_1}/S_{x_jx_1} & S_{x_Lx_2}/S_{x_jx_2} & \cdots & S_{x_Lx_L}/S_{x_jx_L} \end{bmatrix}_{LxL} \tag{7}$$

where (ω) is omitted for convenience. Araújo and Laier [30] proved that the PSDT matrix of Eq. (7) has, at natural frequencies, the unique property of a rank equal to 1 due to linearly dependent columns. Based on this finding, the authors introduced a procedure to identify modal properties by decomposing the matrix through an SVD since the second and the larger singular values tend towards zero if a matrix's rank is 1. Natural frequencies can then be identified from peaks of a graph plotting the inverse of these singular values.

2.3.2. Power spectral density transmissibility & blind source separation

The PSDT technique described above fails to identify closely spaced modes because the matrix of Eq. (7) has, in the proximity of closely spaced modes, a rank larger than 1 due to linearly independent columns. To overcome this problem, Araújo et al. [25] combined the PSDT method and the BSS technique. The BSS technique assumes that the dynamic responses are a combination of sources defined as

$$\mathbf{x}(t) = \mathbf{A}\mathbf{s}(t) \tag{8}$$

where $\mathbf{x}(t)$ is the dynamic response vector, $\mathbf{s}(t)$ is the source vector, and $\mathbf{A}$ represents a static mixing matrix. The aim of the BSS is to decompose the dynamic responses into multiple uncorrelated signals called sources. If linear theory is applicable, a direct relationship exists between BSS and the dynamic responses' modal decomposition given by

$$\mathbf{x}(t) = \mathbf{\Phi}\mathbf{z}(t) \tag{9}$$

where $\mathbf{\Phi}$ is the structure's mode shapes matrix and $\mathbf{z}(t)$ is the response vector in modal coordinates. The similarities between Eqs. (8) and (9) indicate the applicability of BSS for OMA. If BSS decomposes the dynamic responses correctly, the structure's mode shapes can be estimated directly using the mixing matrix.

Araújo et al. [25] suggested using Second Order Blind Identification (SOBI) as a BSS technique [31]. SOBI is applicable to identify closely spaced modes. Moreover, according to Araújo et al. [25], SOBI is the most robust BSS method for non-fully loaded structures (i.e. not all the Degrees Of Freedom (DOFs) of the system are loaded). SOBI defines the mixing matrix $\mathbf{A}$ and, afterwards, estimates the sources by

$$\mathbf{s}(t) = \mathbf{A}^{-1}\mathbf{x}(t) \tag{10}$$

and obtains the contribution of source q at all sensor locations by

$$a_i^q(t) = \mathbf{A}(i,q)s_q(t) \tag{11}$$

where $s_q(t)$ is source q and $a_i^q(t)$ is the contribution of source q at sensor location i. Araújo et al. [25] proposed to incorporate the obtained sources in a new PSDT matrix given by

$$\left[\mathbf{PT}_j^q(\omega)\right] = \begin{bmatrix} S_{x_1x_1}/S_{a_j^q a_1^q} & S_{x_1x_2}/S_{a_j^q a_2^q} & \cdots & S_{x_1x_L}/S_{a_j^q a_L^q} \\ S_{x_2x_1}/S_{a_j^q a_1^q} & S_{x_2x_2}/S_{a_j^q a_2^q} & \cdots & S_{x_2x_L}/S_{a_j^q a_L^q} \\ \vdots & \vdots & \ddots & \vdots \\ S_{x_Lx_1}/S_{a_j^q a_1^q} & S_{x_Lx_2}/S_{a_j^q a_2^q} & \cdots & S_{x_Lx_L}/S_{a_j^q a_L^q} \end{bmatrix}_{LxL} \tag{12}$$

The authors proved that the PSDT matrix of Eq. (12) contains only one natural frequency, corresponding to the vibration mode of source q and demonstrated that the matrix has the unique property of a rank equal to 1 at the natural frequency. Therefore, the modal properties of the vibration mode of source q can be identified as prescribed by Araújo and Laier [30]. The structure's modal properties, including the closely spaced modes, are subsequently obtained by performing this for multiple sources (i.e. $q = 1, \ldots, L$).

However, the PSDT & BSS method encounters some limitations in identifying modal properties. The PSDT & BSS method misidentifies modal properties if: (1) deficient separation of sources occurs because the number of active modes is larger than the number of sensors [25]; (2) deficient separation of sources occurs because the structure is non-fully loaded [25]; (3) spurious modes are introduced by the PSDT & BSS method because the structure is non-fully loaded [27]; and (4) harmonic modes are present because the structure is excited by harmonic loads [26].

2.3.3. Enhanced power spectral density transmissibility

Araújo et al. [27] propose an enhanced PSDT method that recommends a modified PSDT matrix to eliminate possible spurious modes (see point (3) in Section 2.3.2). The modified PSDT matrix is a reduced form of the Moore–Penrose pseudo-inverse of the matrix $\mathbf{T}_j(\omega)$ and is given by

$$\left[\mathbf{T}_j(\omega)\right]^{++} = \sum_{i=1}^{k} \frac{1}{\sigma_i^j(\omega)} \mathbf{V}_i^j(\omega)\mathbf{U}_i^j(\omega)^{*T} \tag{13}$$

where $\sigma_i^j(\omega)$, $\mathbf{V}_i^j(\omega)$ and $\mathbf{U}_i^j(\omega)$ are the ith singular value, right-singular vector, and left-singular vector of $\mathbf{T}_j(\omega)$, and k is the number of singular values used in the summation. The paper of Araújo et al. [27] prescribes a procedure for determining k. After that, to identify modal properties, the authors calculate a weighted average function by

$$\pi(\omega) = \frac{\sum_{j=1}^{L}(\sigma_1^j(\omega))^2}{\sum_{j=1}^{L}(\sigma_1^j(\omega))} \tag{14}$$

where $\sigma_1^j(\omega)$ is the first singular value of the modified PSDT matrix of Eq. (13) and L the number of measurement locations. Modal properties are identified subsequently from peaks of the weighted average graph.

2.3.4. Kurtosis assessment

Do et al. [26] use a post-processing step based on a Kurtosis assessment to deal with harmonic modes (see point (4) in Section 2.3.2). The Kurtosis assessment filters a peak in the frequency domain and transforms the filtered peak back to the time domain to determine the Kurtosis value and the histogram of the filtered peak. The Kurtosis value and histogram indicate if the peak's origin can be attributed to an inherent structural mode or the response of an applied harmonic load [3]. On the one hand, a structural mode has a histogram with a Gaussian distribution shape and a Kurtosis value close to 3 because the dynamic response driven by structural modes tends to be Gaussian for every type of excitation by the central limit theorem. On the other hand, the dynamic response due to a harmonic load has a histogram with in the middle a minimum and at two extremes two maxima and a Kurtosis value of 1.5.

2.3.5. Enhanced procedure of the PSDT & BSS method

This paper proposes the enhanced PSDT & BSS method that incorporates the findings of Do et al. [26] and Araújo et al. [27] in the existing PSDT & BSS method [25] to overcome some of its limitations (see points (3) and (4) in Section 2.3.2). The procedure to identify modal properties using the enhanced PSDT & BSS method is as follows:

1. Assemble the PSDT matrix of Eq. (7) and determine the number of singular values k according to Araújo et al. [27];
2. Perform SOBI [31] to compute the mixing matrix $\mathbf{A}$ and collect $a_i^q(t)$ in line with Eq. (11);
3. Assemble the PSDT matrix of Eq. (12) for source q;
4. Modify the PSDT matrix of step 3 according to Eq. (13) using k defined in step 1;
5. Plot the weighted average function, as defined in Eq. (14), for the modified PSDT matrix of step 4;
6. Select the peaks of the weighted average graph plotted in step 5;
7. Assess if a peak originates from the dynamic response of an inherent structural mode or a harmonic load using the Kurtosis assessment of Do et al. [26];
8. Identify the natural frequency from the peak of the weighted average graph for peaks driven by structural modes according to step 7;
9. Identify the mode shape from the mixing matrix $\mathbf{A}$ for peaks that are driven by structural modes according to step 7;
10. Repeat steps 3 to 9 for all sources (i.e. $q = 1, \ldots, L$).

2.4. Hybrid OMA procedure

Sections 2.2 and 2.3 reveal that both the FDD and the enhanced PSDT & BSS possess advantages and limitations in fulfilling the benchmark criteria of Section 2.1. The FDD method accurately estimates the modal properties as long as the applied loads form an uncorrelated white noise excitation acting over the entire structure. However, this loading assumption is violated by environmental and operational loads acting on an OWT [20], and as a consequence, modal properties may be misidentified. The enhanced PSDT & BSS identification method, explained in Section 2.3.5, has the advantage of being independent of the applied loads, and the approach separates the dynamic response driven by harmonic loads from the dynamic response governed by structural modes. Both capabilities of the enhanced PSDT & BSS method reduce the risk of misidentification of modal properties. The applicability of the enhanced PSDT & BSS method might, despite that, be limited because the approach requires that the number of sensors is larger than the number of active modes and that the structure is a fully loaded structure (see points (1) and (2) in Section 2.3.2).

A second refined transmissibility-based technique is proposed that combines steps of the enhanced PSDT & BSS method and the FDD method to overcome the limitations and still benefit from the advantages of both techniques. The proposed hybrid OMA procedure uses the PSDT method and the Kurtosis assessment to reduce the risk of misidentifications due to non-white noise excitations (see benchmark criteria (3) in Section 2.1) and the FDD method to identify closely spaced modes (see benchmark criteria (1) and (2) in Section 2.1). The FDD method is preferred over the BSS method to identify closely spaced modes since the FDD method is user-friendlier and more robust for non-fully loaded structures. The procedure of the hybrid OMA method is as follows:

1. Perform the FDD and select candidate modal properties according to Section 2.2;
2. Assemble the PSDT matrix of Eq. (7) and determine the number of singular values k according to Araújo et al. [27];
3. Construct the modified PSDT matrix of Eq. (13) using k and the PSDT matrix of step 2;
4. Select peaks of the weighted average graph of Eq. (14);
5. Assess if a peak is driven by an inherent structural mode or by a harmonic load using the Kurtosis assessment of Do et al. [26];
6. Identify the natural frequencies and the mode shapes from the FDD's candidate modal properties of step 1 for peaks governed by structural modes according to step 5.

3. Description of the numerical model

3.1. Governing equations and solution procedure

The Equations Of Motion (EOMs) of the numerical model are expressed in a matrix and compact form as

$$\mathbf{M}(t)\ddot{\mathbf{x}}(t) + \mathbf{C}(t)\dot{\mathbf{x}}(t) + \mathbf{K}\mathbf{x}(t) = \mathbf{S}_p\mathbf{p}(t) \tag{15}$$

where $\mathbf{M}(t)$, $\mathbf{C}(t)$, and $\mathbf{K}$ are the OWT's mass, damping, and stiffness matrices, $\mathbf{S}_p$ and $\mathbf{p}(t)$ represent the applied loads on the OWT, and $\mathbf{x}(t)$ and its time derivatives describe the OWT's oscillatory behaviour. It should be noticed that the matrices $\mathbf{M}(t)$ and, because of the use of proportional damping, $\mathbf{C}(t)$ in Eq. (15) are time-dependent to reproduce the OWT's time-varying structural behaviour properly.

To solve the differential equations, Eq. (15) is converted into a discrete-time state-space model [3], formulated at time step k as

$$\mathbf{s}_{k+1} = \mathbf{A}_k\mathbf{s}_k + \mathbf{B}_k\mathbf{p}_k \tag{16}$$

where $\mathbf{s}_k = \mathbf{s}(k\Delta t)$ is the discrete-time state vector consisting, for a given sampling period Δt, of $\mathbf{x}_k = \mathbf{x}(k\Delta t)$ and $\dot{\mathbf{x}}_k = \dot{\mathbf{x}}(k\Delta t)$, $\mathbf{p}_k = \mathbf{p}(k\Delta t)$ is the sampled applied forcing, $\mathbf{A}_k$ the discrete-time state matrix, and $\mathbf{B}_k$ the discrete-time input matrix. The discrete-time state matrix $\mathbf{A}_k$ and the discrete-time input matrix $\mathbf{B}_k$ are given by

$$\mathbf{A}_k = e^{\mathbf{A}_c(k\Delta t)\Delta t} \tag{17}$$

$$\mathbf{B}_k = (\mathbf{A}_k - \mathbf{I})\mathbf{A}_c(k\Delta t)^{-1}\mathbf{B}_c(k\Delta t) \tag{18}$$

where $\mathbf{A}_c(t)$ and $\mathbf{B}_c(t)$ are the continuous-time state matrix and the continuous-time input matrix, defined as

$$[\mathbf{A}_c(t)] = \begin{bmatrix} \mathbf{0} & \mathbf{I} \\ -\mathbf{M}(t)^{-1}\mathbf{K} & -\mathbf{M}(t)^{-1}\mathbf{C}(t) \end{bmatrix} \tag{19}$$

$$[\mathbf{B}_c(t)] = \begin{bmatrix} \mathbf{0} \\ \mathbf{M}(t)^{-1}\mathbf{S}_p \end{bmatrix} \tag{20}$$

The discrete-time state-space model of Eq. (16) is solved in Python to simulate the two-bladed OWT's dynamic responses. The solver assumes zero initial conditions of the discrete-time state vector $\mathbf{s}_k$ and updates the mass matrix $\mathbf{M}(t)$ and the damping matrix $\mathbf{C}(t)$ at each time step to reproduce the OWT's time-varying behaviour due to the rotating blades. Consequently, the discrete-time state matrix $\mathbf{A}_k$ of Eq. (17) and the discrete-time input matrix $\mathbf{B}_k$ of Eq. (18) are recalculated too at each time step. After completing the simulation, the solver removes the first five minutes to mitigate the transient dynamic effect due to the zero initial conditions and adds artificial noise to the dynamic responses that consider realistic real-world excitation (see LC2 and LC3 in Section 3.3) to mimic the variability of those real-world excitations. The measurement noise is assumed to be Gaussian noise with zero mean and a standard deviation equal to 10% of the simulated dynamic responses' standard deviation. Eventually, dynamic responses of 45 min with a sampling frequency of 10 Hz are generated for three load cases that will be defined in Section 3.3.

3.2. Two-bladed OWT structure

A 3D numerical model of a two-bladed OWT structure is developed in Python to construct the $\mathbf{M}(t)$, $\mathbf{C}(t)$, and $\mathbf{K}$ matrices of Eq. (15). The numerical model is considerably simplified (e.g., by neglecting the soil–structure interaction, the fluid–structure interaction, and the oscillatory behaviour of the blades) in order to isolate the effects of the applied environmental loads and the time-varying inertia (and damping) matrix on the different OMA procedures. The simplified two-bladed OWT structure consists of the OWT's tower, the Rotor-Nacelle Assembly (RNA), the OWT's blades, and a fixed connection to the ground, as shown in Fig. 1. *The NREL offshore 5-MW baseline wind turbine* of Jonkman et al. [32] is used as a reference to obtain the material and the geometrical properties.

The tower is modelled as a clamped cantilever beam of five two-node 3D Timoshenko beam elements [33]. The 3D Timoshenko elements are used to include torsional and, more relevant for this research, closely spaced modes. Each element has the inertial and stiffness properties of a circular hollow steel section of 18 m in length, 6 m in diameter, and 0.027 m in thickness, with a density of 7850 kg/m^3, Young's modulus of 210 GPa, and Poisson's ratio of 0.3. The assembly of five Timoshenko elements discretizes the tower into six nodes. Each node exists of six DOFs: three translational and three rotational DOFs. The DOFs of the bottom node are removed to realize the clamped connection.

The RNA and blades are modelled as a rigid-body mass matrix containing the RNA's and the blades' mass and six inertial contributions. The rigid-body mass matrix is added directly to the top node of the tower, forming a fixed connection able to transfer moment and shear forces. Note that such a fixed connection could be relaxed by introducing a localized rotational stiffness between the tower and the RNA. However, this will introduce an extra DOF that can drastically change the structural dynamic behaviour and, for the time being, falls outside the scope of this paper. The mass is the sum of the weight of the nacelle (240 000 kg), the hub (56 780 kg), and the two blades (together 53 411 kg), which are modelled as solid rectangular steel sections of 63 m in length, 0.45 m in

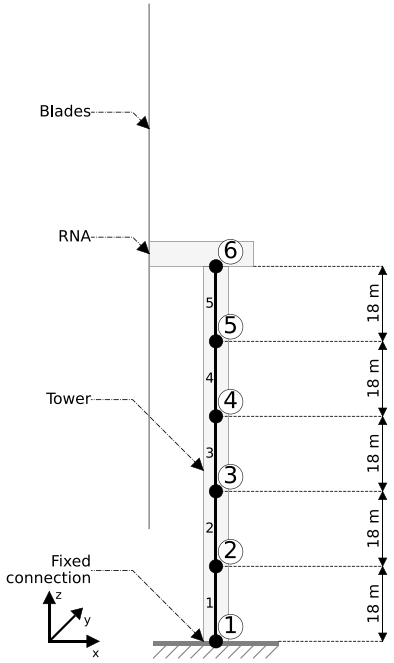

Fig. 1. Simplified two-bladed OWT structure and its elements and nodes.

width, and 0.12 m in thickness, with a density of 7850 kg/m^3, Young's modulus of 210 GPa, and Poisson's ratio of 0.3. The six inertial contributions depend on the RNA's eccentricity (3.5 m) and the time-dependent blades' inertia terms that are calculated by

$$\mathbf{I}_{blades}(t) = \mathbf{R}(t)^T \mathbf{I}_{hor} \mathbf{R}(t) \tag{21}$$

where $\mathbf{I}_{hor}$ is a matrix that contains the blades' inertia terms for the OWT in the horizontal blade configuration, and $\mathbf{R}(t)$ is a time-dependent rotation matrix that is defined as

$$\left[\mathbf{R}(t)\right] = \begin{bmatrix} 1 & 0 & 0 \\ 0 & \cos(\Omega_r t) & -\sin(\Omega_r t) \\ 0 & \sin(\Omega_r t) & \cos(\Omega_r t) \end{bmatrix} \tag{22}$$

where Ω_r is the rotor speed in rad/s of the blades.

The tower elements and the rigid-body mass matrix are assembled to construct the OWT's mass ($\mathbf{M}(t)$) and stiffness ($\mathbf{K}$) matrices. The damping matrix ($\mathbf{C}(t)$) is retrieved using a constant modal damping ratio of 1%, according to the reference OWT of Jonkman et al. [32], for the first five modes. Higher modes are fully damped using a constant modal damping ratio of 100% to decrease the sampling frequency and, subsequently, the computational time. Note, though, that higher modes have been observed during several monitoring campaigns, as discussed in [4–8]. However, this study aims to assess the performance of the proposed OMA procedures for the main structural modes commonly used for design purposes. On top of that, the spectral content of the chosen environmental loads, excluding white noise excitation, does not activate higher modes than the first two (closely spaced) modes (see Sections 3.3 and 4.1). It is also important to stress that any procedure which includes techniques such as BSS requires a number of sensors higher than the number of active modes in the dataset.

The variation of the first five damped natural frequencies for varying blades' azimuthal positions of the two-bladed OWT structure is presented in Fig. 2. It is shown that for changing blades' azimuthal positions, as was previously illustrated by Vergassola et al. [22], the natural frequencies of a two-bladed OWT vary in time, resulting in veering, mode coalescence, and mode shape hybridization phenomena [34,35]. The phenomena of veering and hybridization of modes can clearly be affirmed by investigating the Modal Assurance Criterion (MAC) [36] matrices, as also illustrated in [22]. Fig. 3 provides the MAC matrices for selected azimuthal angles. A comparison of Fig. 3a and f illustrates that various mode shapes switch positions between them, and a glance at Fig. 3b–e exposes a certain level of mode hybridization (e.g., between the bending and the torsional mode).

3.3. Description of the load cases

Three load cases, extensively described in this section and summarized in Table 1, are defined to formulate $\mathbf{S}_p$ and $\mathbf{p}(t)$ of Eq. (15). The three load cases, comprising two standstill OWT configurations and one operative OWT configuration, consider four loading

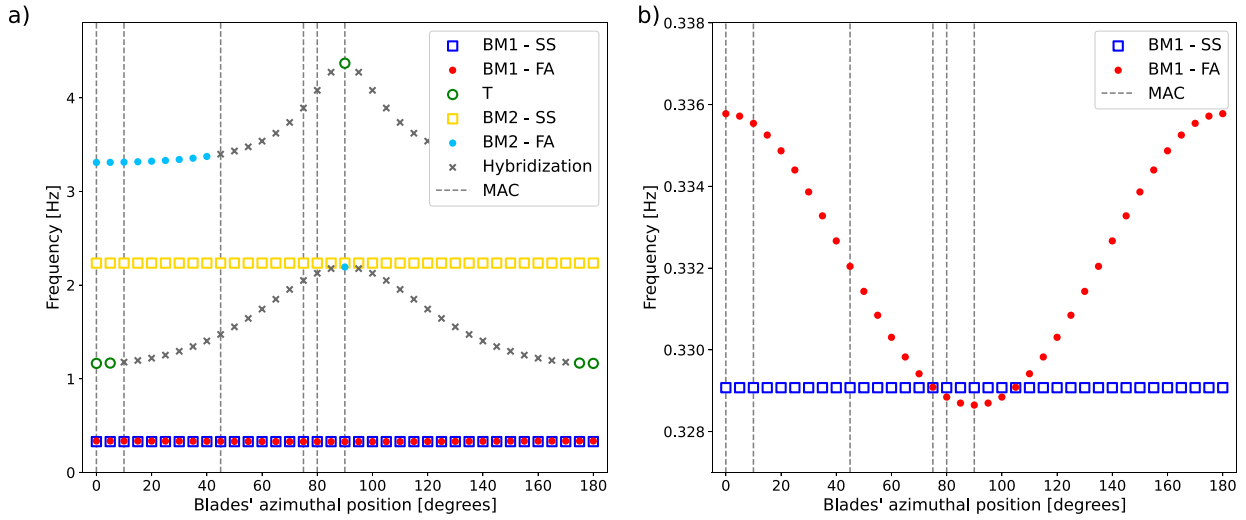

Fig. 2. Damped natural frequencies with respect to the OWT blades' azimuthal position: (a) First five modes; (b) First two bending modes (BM = tower bending mode, T = torsional mode, SS = side-side direction (y-direction in Fig. 1), and FA = fore-aft direction (x-direction in Fig. 1)).

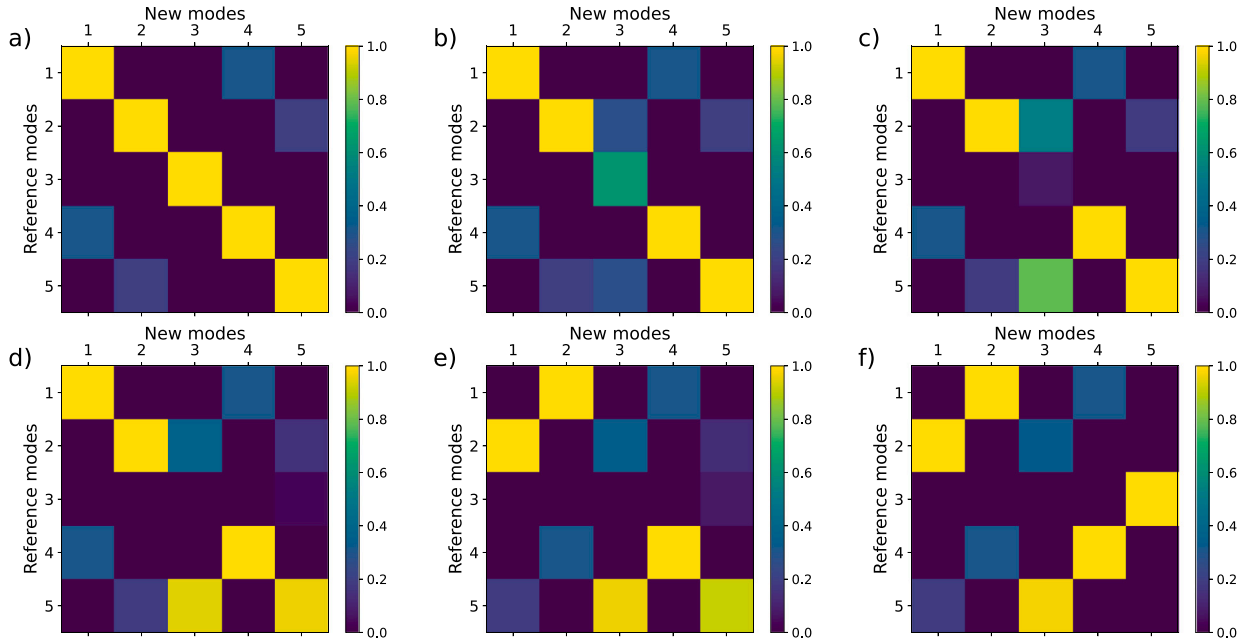

Fig. 3. MAC matrices of the first five modes with reference to a horizontal blade configuration (0°): (a) 0°; (b) 10°; (c) 45°; (d) 75°; (e) 80°; (f) 90°.

Table 1
Description of load cases.

Load case	OWT configuration	Coloured noise excitation	Environmental loads	Operational load
LC1	Standstill	✓	–	–
LC2	Standstill	–	✓	–
LC3	Operative	–	✓	✓

components, presented in Fig. 4, i.e. coloured noise, aerodynamic (due to the wind load), hydrodynamic (due to the wave load), and operational (due to the rotation of the blades).

Load case 1 (LC1) is a theoretical OWT case to validate the implementation of the three OMA-based procedures. The OWT is in the standstill horizontal blade configuration (i.e. 0° as the blades' azimuthal position in Fig. 2) and excited by coloured noise

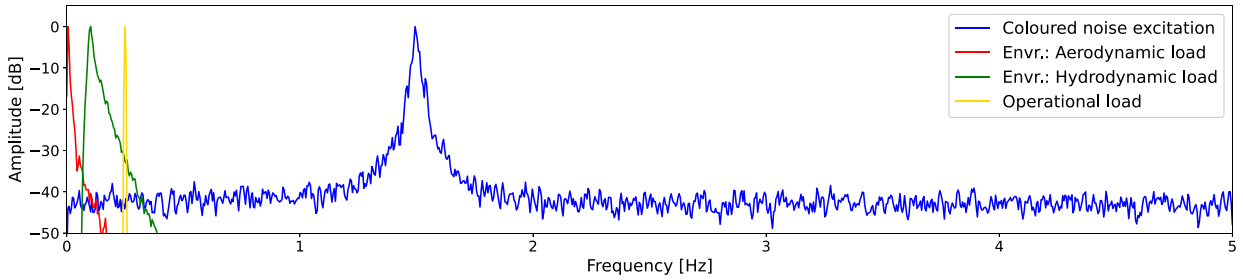

Fig. 4. Spectra normalized by their maximum of coloured noise excitation, environmental loads (aerodynamic and hydrodynamic), and operational load.

sequences, as indicated in Table 1. Uncorrelated coloured noise excitations with an arbitrary predominant frequency of 1.5 Hz load all translational DOFs in the FA and the SS direction and all rotational DOFs around the z-axis. The coloured noise excitations, coupled with the aforementioned frequency, are simulated as the displacement response of a Single DOF (SDOF) system with a mass of 1 kg, a viscous damping coefficient of 0.25 Ns/m, and a spring stiffness of $9\pi^2$ N/m excited by a white noise sequence having a zero mean and 37.5 N standard deviation. Subsequently, white noise with a zero mean and 1.5 N standard deviation is superimposed on the simulated displacement response to create a coloured noise sequence that excites all OWT modes effectively. An example of a spectrum of a generated coloured noise excitation is presented in Fig. 4. The magnitude of the white noise excitation is four times larger in the FA direction than in the SS direction and, to properly excite the torsional modes, 50 times larger around the z-axis than in the FA direction. Appendix A explains why the excitation differs in magnitude in the FA and the SS direction.

Table 1 specifies that load case 2 (LC2) involves a standstill OWT in the horizontal blade configuration (i.e. 0° as the blades' azimuthal position in Fig. 2) excited by environmental (aerodynamic and hydrodynamic) loads that violate OMA's fundamental loading assumptions. Two wind velocity time series are simulated, one in the FA direction and one in the SS direction, using the Kaimal spectrum [37] with a zero mean value, a 10-min mean wind speed of 12 m/s at a reference height of 10 m, and a turbulence intensity of 20%. The mean wind speed of 12 m/s at 10 m is added with a logarithmic profile over the tower's height to the time series in the FA direction. The aerodynamic loads induced by the wind velocity time series are calculated according to DNV-RP-C205 [38], resulting in wind force spectra similar to the aerodynamic spectrum illustrated in Fig. 4. The generated aerodynamic forces are applied to the translational DOFs in the FA and the SS direction of the top four nodes (nodes 3 to 6 in Fig. 1) and to the rotational DOF around the z-axis of node 6 to account for moments introduced by eccentrically loaded blades. In addition, a Morison wave load due to irregular wave states combined with the astronomical tide range equal to 3 m is simulated, assuming an underlying JONSWAP spectrum [37] characterized by a significant wave height equal to 6 m and a peak period of 10 s. The mean water level of the sea is assumed to be at the second node (18 m above the bottom node, see Fig. 1), and the direction of the irregular wave follows the wind velocity's direction. The hydrodynamic load, in terms of a concentrated force, and its point of application are calculated according to DNV-RP-C205 by assuming Stokes' second-order wave theory and Wheeler's stretching method [38]. The computed concentrated hydrodynamic load, of which Fig. 4 shows its spectrum, has a time-varying point of application in the bottom element and is, therefore, applied as time-dependent equivalent nodal forces and nodal moments on node 2 of the bottom element.

Load case 3 (LC3) considers, according to Table 1, an operative OWT excited by operational and environmental loads that both violate OMA's fundamental assumptions. The blades of the two-bladed OWT rotate due to the wind turbine's operative condition, resulting in time-varying modal properties and, in addition, in operational loads caused by a centrifugal force attributed to a mass imbalance of the two blades. The operational loads are harmonic forces of which the magnitude and forcing frequency depend on the mass imbalance, assumed to be 5% of the mass of one blade and located in the middle of the blade, and on the rotor speed, selected to be 15 rpm and constant over time. The harmonic loads, which have similar spectra as the operational load spectrum presented in Fig. 4, are applied to the translational DOFs of the top node of the OWT (node 6) and, because of the RNA's eccentricity, also to rotational DOFs of node 6. The environmental loads are the aerodynamic and hydrodynamic loads described in the previous load case. The aerodynamic load is, however, slightly modified in the FA direction by including a time-dependent shielding factor since rotating blades obstruct wind loads to excite the tower continuously (i.e. the blade passing effect of an operative OWT).

4. Dynamic identification results

4.1. Analysis procedure

The dynamic identification algorithms are applied on the FA and the SS displacements, along with the rotations around the z-axis of nodes 2 to 6 visualized in Fig. 1, aiming to identify all modes for LC1 and the first two (closely spaced) modes for LC2 and LC3. Identification of higher modes for LC2 and LC3 is not considered since higher modes of the wind turbine tower (and support structure) are hardly excited due to the definition of the applied environmental and operational loads modelled according to the DNV-RP-C205 [38] design code with no spectral content at higher frequencies, as illustrated in Fig. 4.

The modal identification results for LC1 and LC2 are compared with the known modelled modal properties of the horizontal blade configuration (i.e. 0° as the blades' azimuthal position in Fig. 2). The OMA-based procedures assume, to perform the modal identification, that LC3 is a linear time-invariant system, despite the fact that LC3 is a linear time-variant system due to the OWT's time-varying modal properties. The identified frequencies are, as a result, a coalescence of the time-varying natural frequencies presented in Fig. 2. On the other hand, the identified closely spaced mode shapes are, when correctly identified, identical to the modelled closely spaced mode shapes since Fig. 2b and the MAC matrices in Fig. 3 demonstrate that the mode shapes of BM1-FA and BM1-SS remain constant over time. This behaviour of the closely spaced mode shapes is used to compare the modal identification results for LC3 with corresponding known modelled modal properties of both the horizontal and vertical blade configuration (i.e. 0° and 90° as the blades' azimuthal position in Fig. 2) to assess the influence of the time-variation of the modal properties on OMA procedures.

To clarify the data processing, the OMA-based procedures calculate the auto/cross — PSD matrices by Welch's method using a Fourier transform of size 2^{11}, 50% overlap, and a Hamming window of size 2^{11}. One last remark is that the numerical analysis carried out for this study uses four digits after the decimal to separate the closely spaced modes (especially for the vertical blade configuration, i.e. 90° as the blades' azimuthal position in Fig. 2). Similarly, the OMA results consider four digits also, although four digits are inappropriate for OMA since such accuracy can, in reality, hardly be obtained.

4.2. Frequency domain decomposition

The results in Tables 2, 3, and 4 and Figs. 5 and 6 demonstrate that the FDD method can identify all excited modes of the two-bladed OWT for all three LCs, even the closely spaced modes. The identified natural frequencies are close to the modelled natural frequencies, and the MAC values prove that the FDD method accurately estimates the mode shapes. However, the FDD method identifies additional peaks that do not belong to modal properties, like the 1.5 Hz coloured noise peaks for LC1 in Table 2 and Fig. 5, the environmental load peaks for LC2 in Table 3 and Fig. 6a, and the operational load peaks for LC3 in Table 4 and Fig. 6b. Hence, it is evident that the FDD results are corrupted by the violation of the OMA fundamental assumptions, leading to unreliable results for field application if the exact structural modes are not known a priori.

Table 2
Numerical results for LC1 by using the FDD.

Mode	Natural frequency [Hz]		Error [%]	MAC [–]
	Modelled	Identified		
BM1 - SS	0.3291	0.3271	0.59	0.98
BM1 - FA	0.3358	0.3369	0.33	1.00
T	1.1641	1.1670	0.25	1.00
[a]	–	1.4941	–	–
[a]	–	1.4990	–	–
BM2 - SS	2.2350	2.2412	0.28	1.00
BM2 - FA	3.3100	3.3057	0.13	1.00

[a] Misidentification of a non-structural mode.

Table 3
Numerical results for LC2 by using the FDD.

Mode	Natural frequency [Hz]		Error [%]	MAC [–]
	Modelled	Identified		
[a]	–	0.0977	–	–
[a]	–	0.1047	–	–
BM1 - SS	0.3291	0.3271	0.59	1.00
BM1 - FA	0.3358	0.3369	0.33	1.00

[a] Misidentification of a non-structural mode.

Table 4
Numerical results for LC3 by using the FDD.

Mode	Natural frequency [Hz]			MAC [–]
	Horizontal	Vertical	Identified	
[a]	–	–	0.2490	–
[a]	–	–	0.2539	–
BM1 - SS	0.3291	0.3291	0.3271	0.99
BM1 - FA	0.3358	0.3286	0.3320	1.00

Horizontal and vertical refer to the modelled horizontal (0°) and vertical (90°) blade configuration.
[a] Misidentification of a non-structural mode.

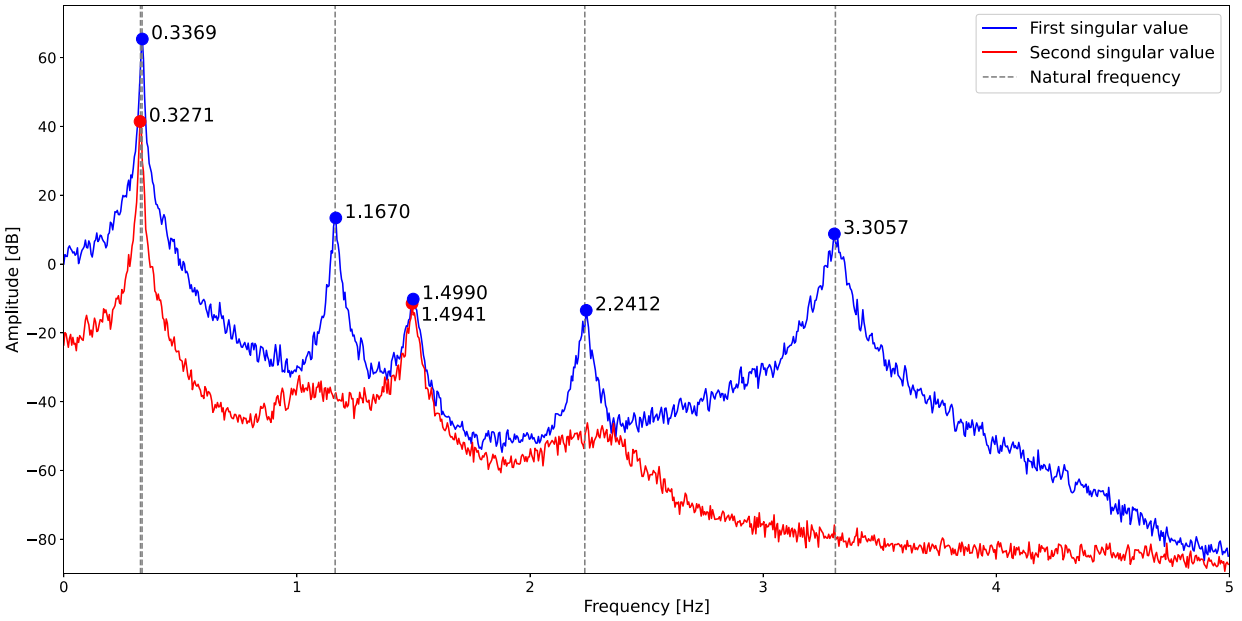

Fig. 5. Numerical results for LC1 by using the FDD.

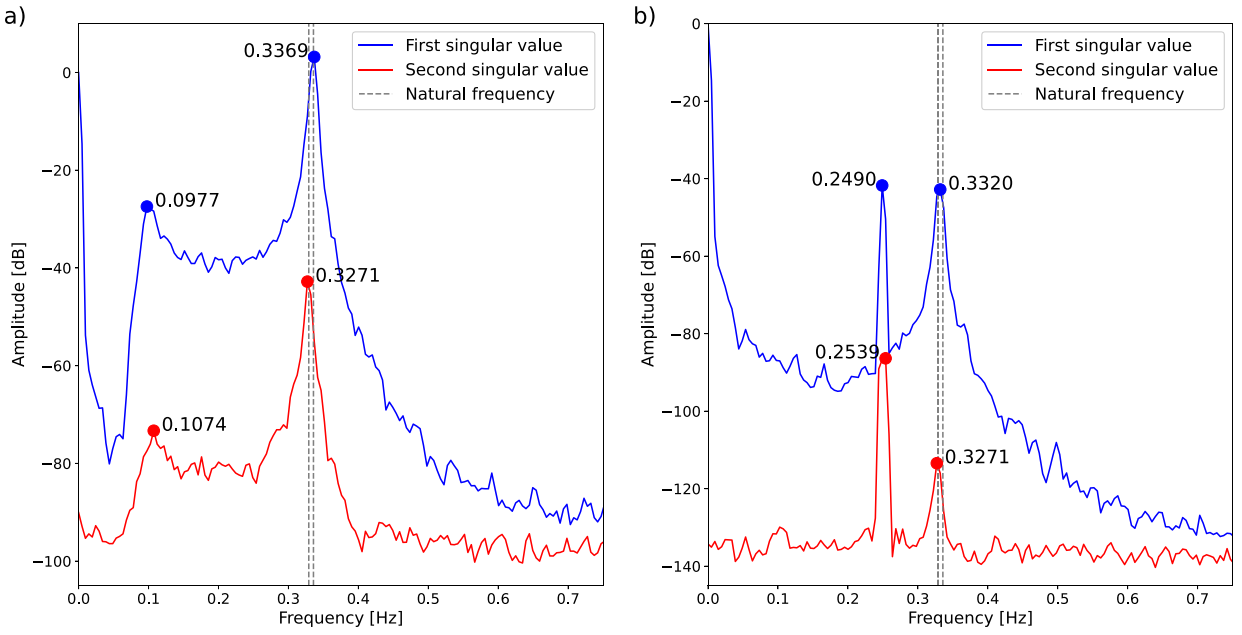

Fig. 6. Numerical results by using the FDD: (a) LC2; (b) LC3.

4.3. Enhanced PSDT & BSS method

Table 5 and Fig. 7 prove that the enhanced PSDT & BSS method identifies all excited modes of the two-bladed OWT for LC1. The identified natural frequencies are close to the modelled natural frequencies, and the estimated mode shapes are accurate. Besides, the results are independent of the coloured noise excitation. The PSDT & BSS method does not identify an additional peak around 1.5 Hz like the FDD method in Fig. 5.

However, Tables 6 and 7 and Fig. 8 show that the enhanced PSDT & BSS method identifies additional peaks for LC2 and LC3, like the environmental load peaks around 0.10 Hz and the operational load peak close to 0.25 Hz. The PSDT & BSS method cannot remove these peaks since the loads' spectra are non-wideband, as shown in Fig. 4 and as explained in [39]. Therefore, to overcome

Table 5
Numerical results for LC1 by using the enhanced PSDT & BSS.

Mode	Natural frequency [Hz]		Error [%]	Kurtosis [–]	MAC [–]
	Modelled	Identified			
BM1 - SS	0.3291	0.3271	0.59	2.97	0.99
BM1 - FA	0.3358	0.3369	0.33	3.04	1.00
T	1.1641	1.1621	0.17	2.74	1.00
BM2 - SS	2.2350	2.2266	0.38	3.18	1.00
BM2 - FA	3.3100	3.2861	0.72	3.00	1.00

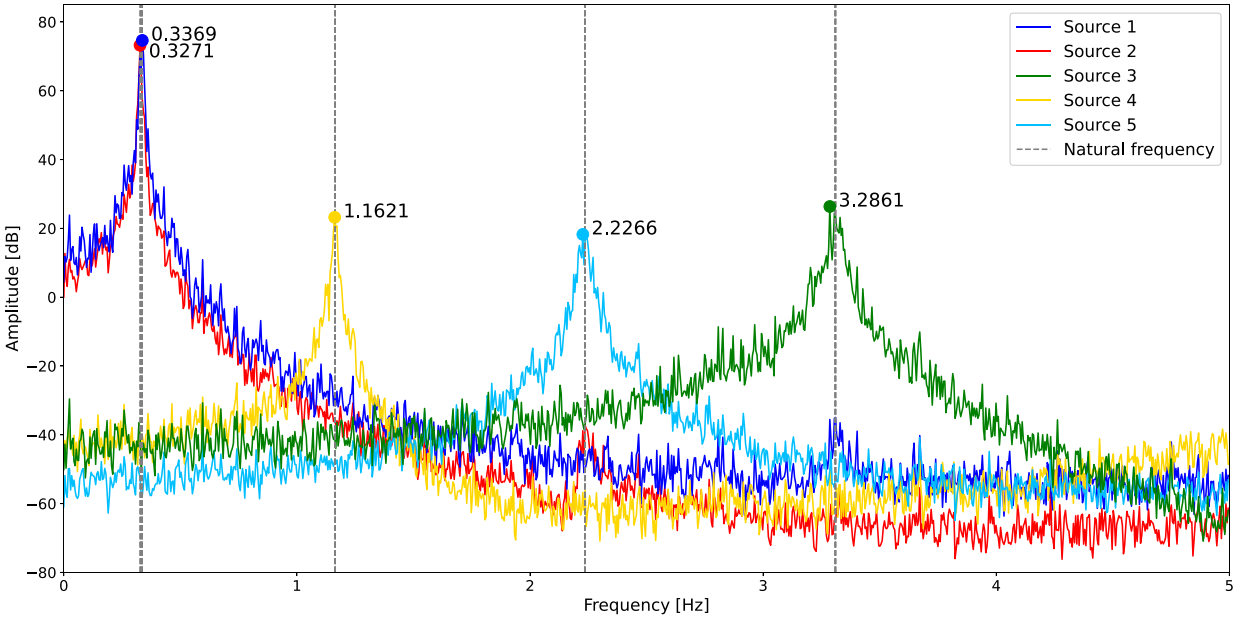

Fig. 7. Numerical results for LC1 by using the enhanced PSDT & BSS.

this intrinsic limitation of the enhanced PSDT & BSS, the Kurtosis value of the recorded displacements and rotations is used to assess whether a peak corresponds to the activation of a structural mode or the dynamic response of an applied harmonic load, as suggested by Do et al. [26]. The Kurtosis value of 1.5, reported in Table 7 for the peak at 0.249 Hz, shows that this technique is able to distinguish between a structural mode peak and an operational/harmonic load peak. However, the Kurtosis values between 2.7 and 2.8, shown in Tables 6 and 7, attributed to the environmental load peaks, show that even the Kurtosis value assessment misidentifies such peaks as structural modes.

Moreover, Table 6 shows an incorrect mode shape estimation of BM1-SS for LC2 due to a non-fully loaded condition (see (2) in Section 2.3.2), i.e. the magnitude of the applied excitation in the SS direction is negligible in comparison to the magnitude in the FA direction (especially for the aerodynamic load).

A crucial remark concerning the use of the enhanced PSDT & BSS method is that, in this research, the applicability of this method is not limited by an insufficient number of sensors. BSS requires, for a proper application, that the number of sensors should be larger than the number of active modes to have sufficient separation of sources. All along this work, the dynamic responses of fifteen DOFs have been adopted (see Section 4.1) as fifteen virtual sensors, while the maximum number of active modes is five (see Section 3.2).

Table 6
Numerical results for LC2 by using the enhanced PSDT & BSS.

Mode	Natural frequency [Hz]		Error [%]	Kurtosis [–]	MAC [–]
	Modelled	Identified			
[a]	–	0.0977	–	2.71	–
[a]	–	0.0977	–	2.71	–
BM1 - SS	0.3291	0.3271	0.59	3.42	0.63
BM1 - FA	0.3358	0.3369	0.33	3.09	1.00

[a] Misidentification of a non-structural mode.

Table 7
Numerical results for LC3 by using the enhanced PSDT & BSS.

Mode	Natural frequency [Hz]			Kurtosis [–]	MAC [–]
	Horizontal	Vertical	Identified		
[a]	–	–	0.0928	2.78	–
[b]	–	–	0.2490	1.50	–
BM1 - SS	0.3291	0.3291	0.3320	3.11	1.00
BM1 - FA	0.3358	0.3286	0.3320	2.94	1.00

Horizontal and vertical refer to the modelled horizontal (0°) and vertical (90°) blade configuration.
[a] Misidentification of a non-structural mode.
[b] Identification of a dynamic response triggered by a harmonic load through the Kurtosis assessment.

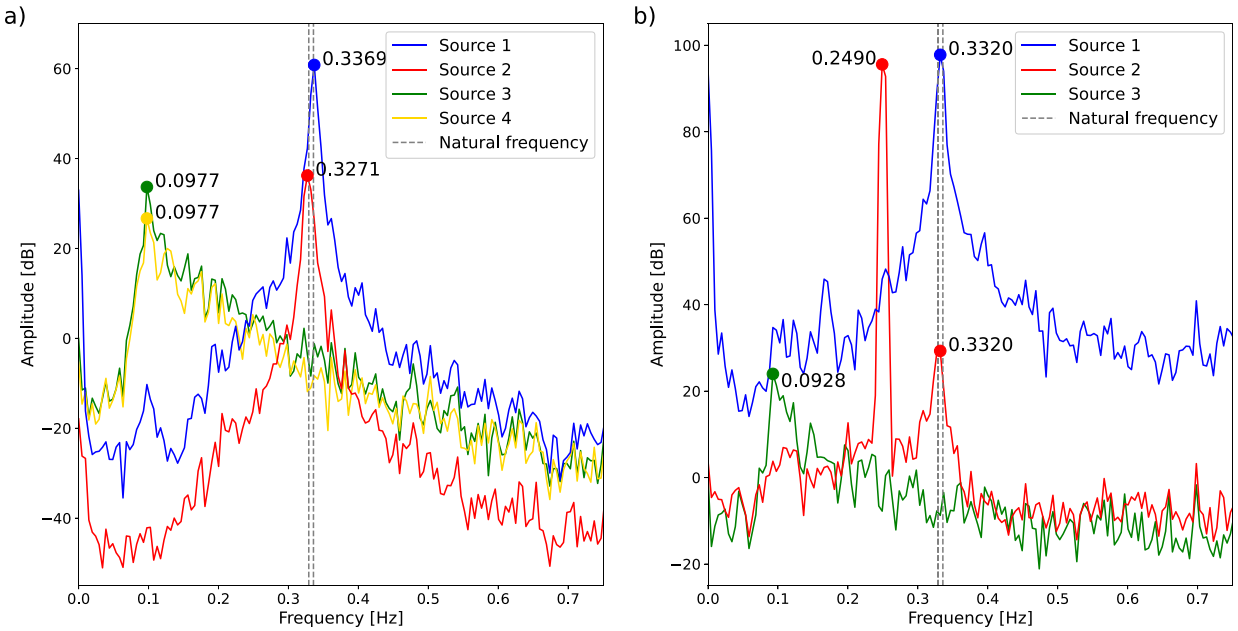

Fig. 8. Numerical results by using the enhanced PSDT & BSS: (a) LC2; (b) LC3.

4.4. Hybrid OMA method

The results in Tables 8, 9 and 10 and Figs. 9, 10, and 11 prove that the hybrid OMA method can identify all excited modes of the two-bladed OWT for all three LCs. The identified natural frequencies are close to the modelled natural frequencies. Moreover, in contrast to the enhanced PSDT & BSS method, the hybrid OMA method obtains accurate estimations for all mode shapes, even for BM1-SS of LC2, since the FDD method is used to estimate the mode shapes. The results for LC1 are independent of the coloured noise excitation since the PSDT method removes this peak, as shown in Table 8 and Fig. 9. For LC3, the hybrid OMA method

Table 8
Numerical results for LC1 by using the hybrid OMA.

Mode	Natural frequency [Hz]		Error [%]	Kurtosis [–]	MAC [–]
	Modelled	Identified			
BM1 - SS	0.3291	0.3271	0.59	3.04	0.98
BM1 - FA	0.3358	0.3369	0.33	3.04	1.00
T	1.1641	1.1670	0.25	2.74	1.00
[a]	–	1.4941	–	–	–
[a]	–	1.4990	–	–	–
BM2 - SS	2.2350	2.2412	0.28	3.18	1.00
BM2 - FA	3.3100	3.3057	0.13	3.00	1.00

[a] Peak removed by PSDT.

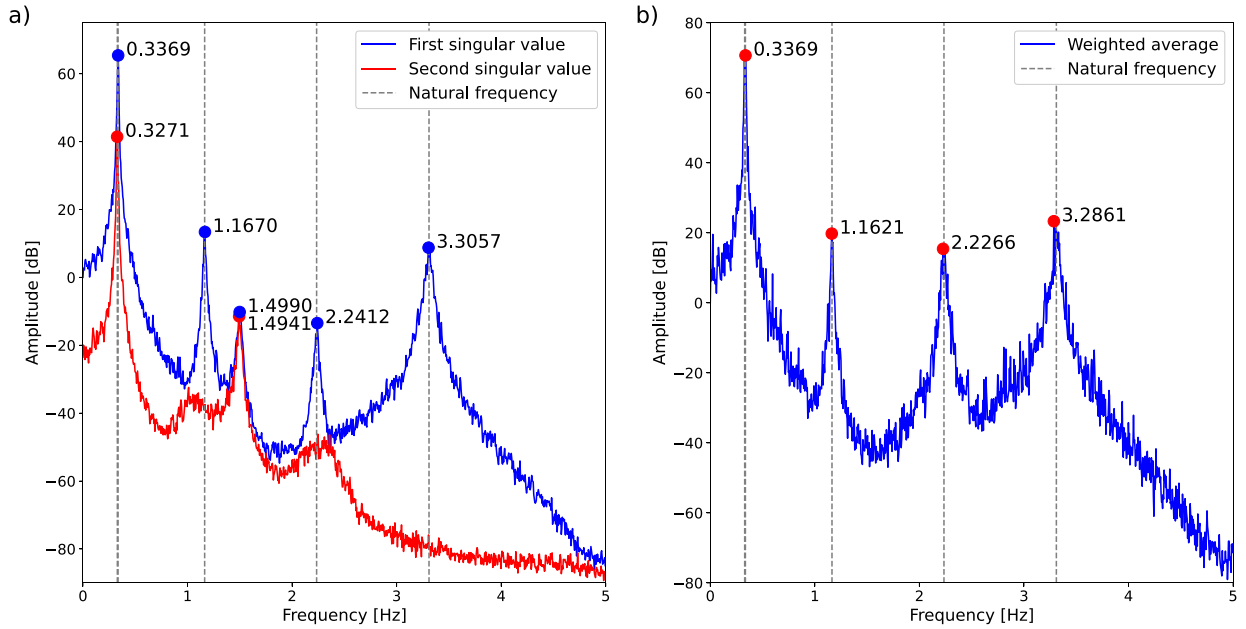

Fig. 9. Numerical results for LC1 by using the hybrid OMA: (a) FDD; (b) PSDT.

Table 9
Numerical results for LC2 by using the hybrid OMA.

Mode	Natural frequency [Hz]		Error [%]	Kurtosis [–]	MAC [–]
	Modelled	Identified			
[a]	–	0.0977	–	2.71	–
[a]	–	0.1074	–	2.71	–
BM1 - SS	0.3291	0.3271	0.59	3.09	1.00
BM1 - FA	0.3358	0.3369	0.33	3.09	1.00

[a] Misidentification of a non-structural mode.

Table 10
Numerical results for LC3 by using the hybrid OMA.

Mode	Natural frequency [Hz]			Kurtosis [–]	MAC [–]
	Horizontal	Vertical	Identified		
[a]	–	–	0.2490	1.50	–
[a]	–	–	0.2539	1.50	–
BM1 - SS	0.3291	0.3291	0.3271	2.94	0.99
BM1 - FA	0.3358	0.3286	0.3320	2.94	1.00

Horizontal and vertical refer to the modelled horizontal (0°) and vertical (90°) blade configuration.
[a] Identification of a dynamic response triggered by a harmonic load through the Kurtosis assessment.

separates dynamic responses driven by harmonic loads close to 0.25 Hz from dynamic responses governed by structural modes using the Kurtosis assessment, as shown in Table 10.

Despite the good performance of this proposed method, the hybrid OMA method misidentifies modal properties for LC2 due to environmental loads, as shown in Table 9 and Fig. 10 by the additional peaks close to 0.10 Hz. The PSDT method cannot remove the peak of the non-wideband hydrodynamic spectrum, and the Kurtosis assessment cannot indicate the peak as a non-structural mode.

4.5. Summary OMA results

The results of Sections 4.2, 4.3, and 4.4 are summarized in Table 11 and highlight that the FDD and the enhanced PSDT & BSS have possibilities and limitations in identifying the modal properties of an operative two-bladed OWT. The FDD method accurately estimates the modal properties of the two-bladed OWT as long as there is pre-knowledge of applied excitations since it lacks the capability to distinguish between structural and applied load peaks (see benchmark criteria (3) in Section 2.1). The enhanced PSDT & BSS method has, in contrast to the FDD method, the advantage of being independent of applied wideband and harmonic loads but

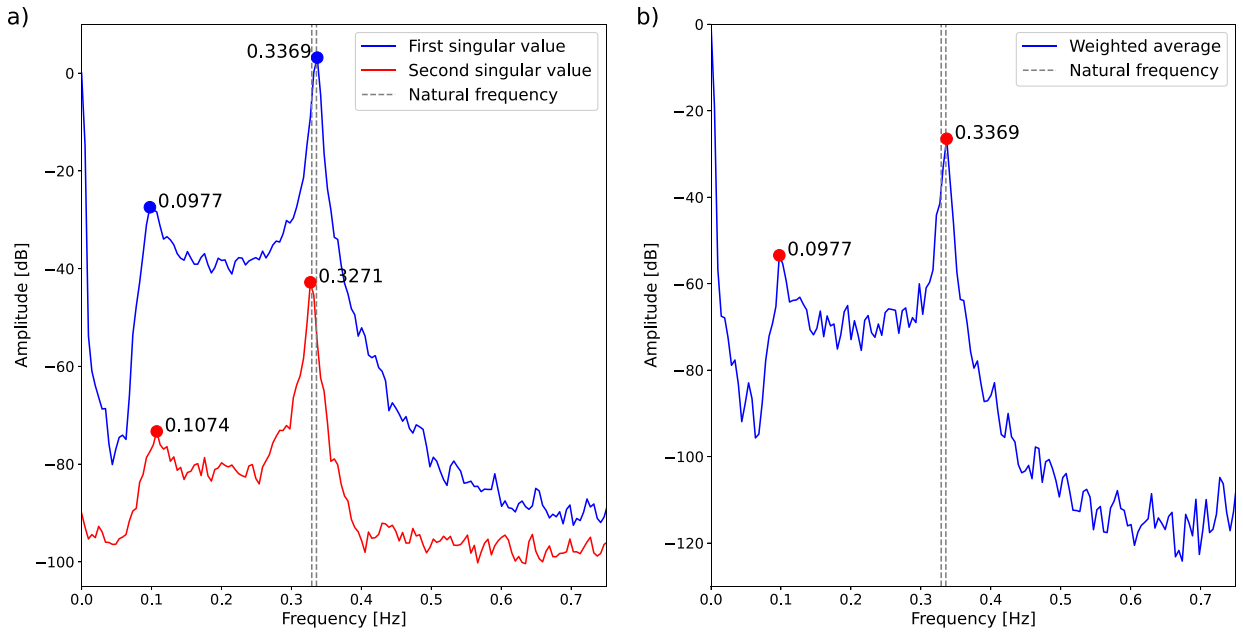

Fig. 10. Numerical results for LC2 by using the hybrid OMA: (a) FDD; (b) PSDT.

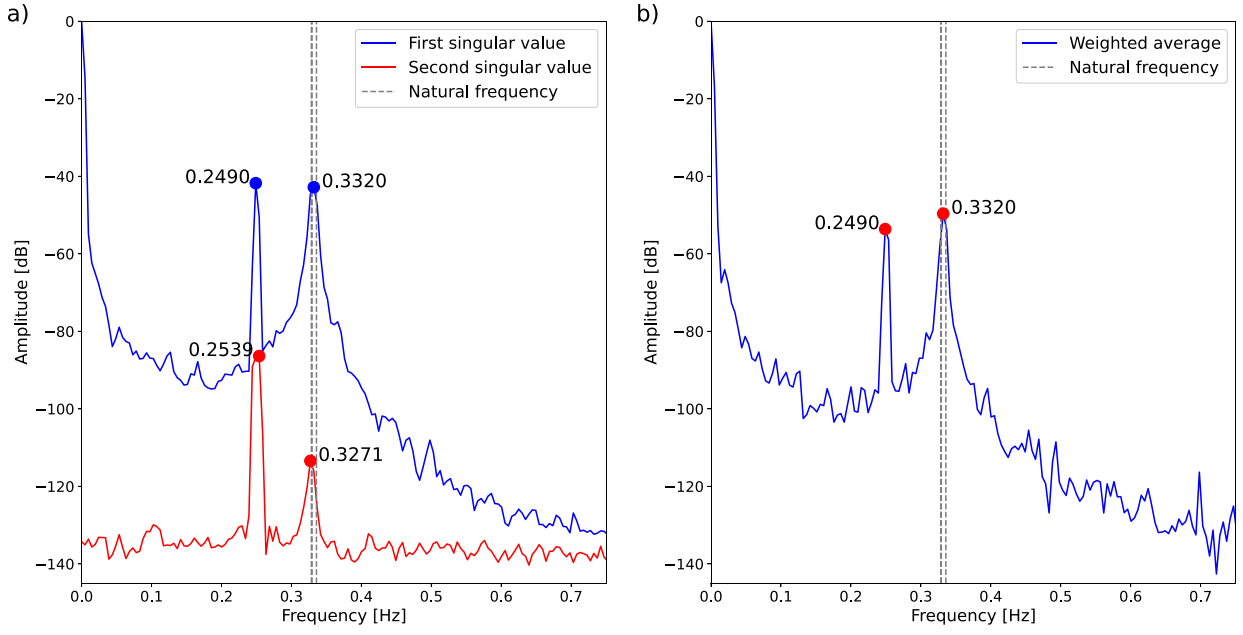

Fig. 11. Numerical results for LC3 by using the hybrid OMA: (a) FDD; (b) PSDT.

Table 11
Overview of the results of the OMA-based procedures with reference to the chosen benchmark criteria.

Benchmark criteria	FDD	Enhanced PSDT & BSS	Hybrid OMA
(1) Natural frequency	✓	✓	✓
(2) Mode shape	✓	–	✓
(3) Wideband excitation	–	✓	✓
(3) Non-wideband excitation	–	–	–
(3) Harmonic excitation	–	✓	✓

requires a fully loaded structure for the correct identification of modal properties (see benchmark criteria (1) and (2) in Section 2.1). On top of that, Table 11 proves that the hybrid OMA procedure outperforms the FDD and the enhanced PSDT & BSS methods by combining the advantages of both techniques. The hybrid OMA procedure surpasses the FDD and the enhanced PSDT & BSS methods because it is independent of applied wideband and harmonic loads and can correctly identify modal properties for non-fully loaded structures. Nevertheless, one drawback remains that even the hybrid OMA method fails to separate the hydrodynamic load peaks from structural modes due to the excitation's non-wideband (and non-harmonic) spectrum.

Another important finding is that the time-varying modal properties of an operative two-bladed OWT are not a limitation for applying the methods. The identified natural frequencies for LC3 using the three methods are, despite resulting in a coalescence (see Section 4.1), an appropriate approximation of the OWT's time-varying natural frequencies since those identified closely spaced modes experience only minor natural frequency fluctuations over time (see Fig. 2b). The mode shapes of these closely spaced modes are, in addition, also accurately identified.

5. Discussion and conclusions

5.1. Discussion

Despite outperforming the FDD and the enhanced PSDT & BSS methods, the hybrid OMA procedure misidentifies modal properties of an OWT due to the hydrodynamic load. To distinguish peaks generated by hydrodynamic loads from peaks governed by structural modes, an additional brief analysis that investigates the identified mode shapes is performed. The identified mode shapes for LC2 by using the hybrid OMA are compared with the modelled mode shapes using the MAC matrix displayed in Fig. 12. The MAC matrix discloses that the MAC index cannot allow a correct interpretation of such non-structural modes since their mode shapes are almost identical to the modelled (closely spaced) mode shapes. This finding can be explained by the fact that an applied (environmental) load with a frequency of excitation below the first natural frequency activates a stiffness-dominated (quasi-static) regime, generating an operational deflective shape which may resemble the shape of the first bending mode of the investigated structure.

A more pragmatic solution to cope with these hydrodynamic loads can be sought by taking advantage of the higher variability over time of the hydrodynamic peak in comparison to the structural mode's peak. For example, field measurements from a 3.6 MW OWT located at the DanTysk wind farm (see [8] for more details) allowed Kjeld et al. to collect the mean wave periods hitting the OWT through a meteorological mast for a period of 491 days. Over 70 770 measured 10-min data blocks were analysed, and results show (see Fig. 4 in [8]) that a detectable hydrodynamic wave frequency can vary between 0.1 to 0.5 Hz, with the highest waves observable at 0.1 Hz. This observation may suggest that, during a long-term dynamic monitoring campaign, the variability of an observed peak may help reveal the peak's structural or non-structural nature. Further investigations may test this hypothesis and support the hybrid OMA procedure to distinguish between non-structural (environmental) peaks and peaks governed by a structural mode.

Next to potential misidentifications due to hydrodynamic loads, two further limitations of the hybrid OMA procedure that are observed should be addressed before considering a broader application. The first shortcoming of the hybrid OMA method (or any

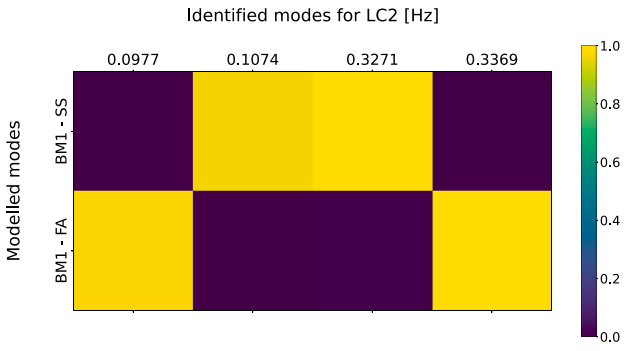

Fig. 12. MAC matrix comparing the modelled mode shapes and the identified mode shapes for LC2 by using the hybrid OMA procedure (see Table 9).

other OMA technique that assumes a linear time-invariant system) is that the violated assumption of a linear time-invariant system can induce damping ratio estimations of the operative two-bladed OWT that are significantly different than the actual damping ratios. Damping ratio estimations higher than the actual damping are likely to be obtained since multiple harmonics belonging to the same structural mode can be observed, causing a final peak in the PSD (adopted to estimate the damping) having a larger width due to the averaging procedure applied over the recorded time series. Another drawback of the hybrid OMA method is that its applicability can be hindered due to applied excitations having a forcing frequency in the proximity of structural modes since studies in the literature show (e.g., [26]) that a structural mode can be hidden by the harmonics of an applied excitation with a forcing frequency close to a natural frequency. In the short term, future work may explore a wider parameter space for the load cases (see Section 3.3) and systematically map the regions of such parameter space in which the hybrid OMA procedure succeeds or not in the dynamic identification process to address this last limitation.

Furthermore, this study focuses on the identification of the first two (closely spaced) modes of an operative two-bladed OWT. Higher modes of the operative OWT are disregarded, even though they may be observed during field monitoring campaigns, as noticed in Section 3.2 and discussed in [4–8]. On the one hand, the identification of higher modes might be needed if the damage sensitivity of the vibration-based SHM procedures needs to be increased. On the other hand, the identification of lower modes can be sufficient for a preliminary model updating exercise, a design process validation, or the detection of global structural variations due to changing boundary conditions. The absence of higher modes in the dynamic responses of the investigated numerical model described in Section 3 is caused by the definition of the applied loads modelled according to the DNV-RP-C205 [38]. Since higher modes have been detected in collected field data [4–8], this could expose eventual shortcomings of the environmental load prescriptions taken from the aforementioned design codes.

The eventual introduction of higher modes may pose further challenges to the hybrid OMA procedure. Section 4.5 concludes that the time-varying structural behaviour of an operative OWT does not affect the modal identification of the closely spaced modes. However, this is true for the first mode, whereas a problem might arise when higher modes are studied. The modal identification process of higher modes can become more challenging because the mode shapes of higher modes do not remain constant over time due to mode hybridization, as demonstrated in Fig. 2a and the MAC matrices in Fig. 3.

5.2. Conclusions

Intending to identify modal properties from two-bladed OWT measurements, this research compares three OMA-based procedures: (1) the standard FDD method; (2) the proposed enhanced PSDT & BSS method that incorporates a post-processing technique based on the Kurtosis index; and (3) the proposed hybrid OMA method that combines the PSDT method, the dedicated post-processing technique based on the Kurtosis index, and the FDD method.

This research proves that the performance of the proposed hybrid OMA method outperforms the FDD and the enhanced PSDT & BSS approaches in identifying the modal properties from dynamic responses generated by a representative numerical model of a two-bladed OWT for three load cases. Compared to the FDD method, the hybrid OMA method reduces the possibility of misidentification in the presence of harmonic or coloured noise excitation. Moreover, unlike the enhanced PSDT & BSS method, the hybrid OMA method correctly estimates the mode shapes for non-fully loaded structures. One drawback is that loads having a non-wideband spectrum, typical for environmental loads, may be identified as modal properties and limit the use of the hybrid OMA method.

Overall, it is evident from this work that exploiting the advantages of multiple OMA approaches is an attractive and promising direction to obtain robust modal identification results since, in this way, challenges can be tackled that cannot be overcome by the individual techniques involved.

CRediT authorship contribution statement

Daan Willem Berend ter Meulen: Data curation, Formal analysis, Investigation, Methodology, Software, Visualization, Writing – original draft. **Alessandro Cabboi:** Conceptualization, Resources, Supervision, Writing – review & editing. **Alessandro Antonini:** Conceptualization, Resources, Supervision, Writing – review & editing.

Declaration of competing interest

The authors declare that they have no known competing financial interests or personal relationships that could have appeared to influence the work reported in this paper.

Data availability

Data will be made available on request.

Acknowledgements

The authors thank Dr. Alice Cicirello for many helpful discussions and contributions towards this research. This research did not receive any specific grant from funding agencies in the public, commercial, or not-for-profit sectors.

Appendix A. Loads in the FA and the SS direction

The loads applied to the OWT differ in magnitude in the FA and the SS direction for all load cases, e.g., the coloured noise magnitude is four times larger in the FA direction than in the SS direction. This appendix explains that the need for using a limited data length causes this difference in magnitude.

Welch's method is used to estimate auto/cross — PSD matrices [3]. The sampling frequency, the segment length, the number of segments, and the overlap between two segments are critical components of Welch's method. Systematically applied during this research is a sampling frequency equal to 10 Hz, a 50% overlap, and a minimum of 25 segments.

In addition, the sensitivity of the FDD results to different segment lengths is investigated to assess its effects on the identified modal properties. Modal properties are identified from dynamic responses of the standstill horizontal blade OWT configuration (i.e. 0° as the blades' azimuthal position in Fig. 2). Fifteen uncorrelated white noise excitations are applied to load the OWT to all translational DOFs in the FA and the SS direction and all rotational DOFs around the z-axis of Fig. 1. The translational white noise excitations have a zero mean and 100 N standard deviation. The rotational white noise excitations also have a zero mean and a 5000 N standard deviation to excite the torsional modes properly.

A reliable identification of the reference modal properties of the horizontal blade OWT configuration (i.e. 0° as the blades' azimuthal position in Fig. 2) is used as a criterion to set up the segment length. A minimum of 2^{11} data points is required to separate the closely spaced modes for a sampling frequency of 10 Hz. Consequently, a dataset of 45 min is required to have 25 averages that overlap 50%. Table A.1 and Fig. A.1 show the modal identification results using a 45-min dataset and 2^{11} data points. Table A.1 and Fig. A.1 expose that the closely spaced modal identification is not as expected. The bending mode in the side-side direction of the closely spaced modes (BM1-SS) has a biased mode shape estimation. Hence, a higher frequency resolution is required to distinguish the closely spaced modes.

Table A.1
Modal identification using 2^{11} data points.

Mode	Natural frequency [Hz]		Error [%]	MAC [–]
	Modelled	Identified		
BM1 - SS	0.3291	0.3320	0.89	0.41
BM1 - FA	0.3358	0.3369	0.33	1.00
T	1.1641	1.1719	0.67	1.00
BM2 - SS	2.2350	2.2363	0.06	1.00
BM2 - FA	3.3100	3.3203	0.31	1.00

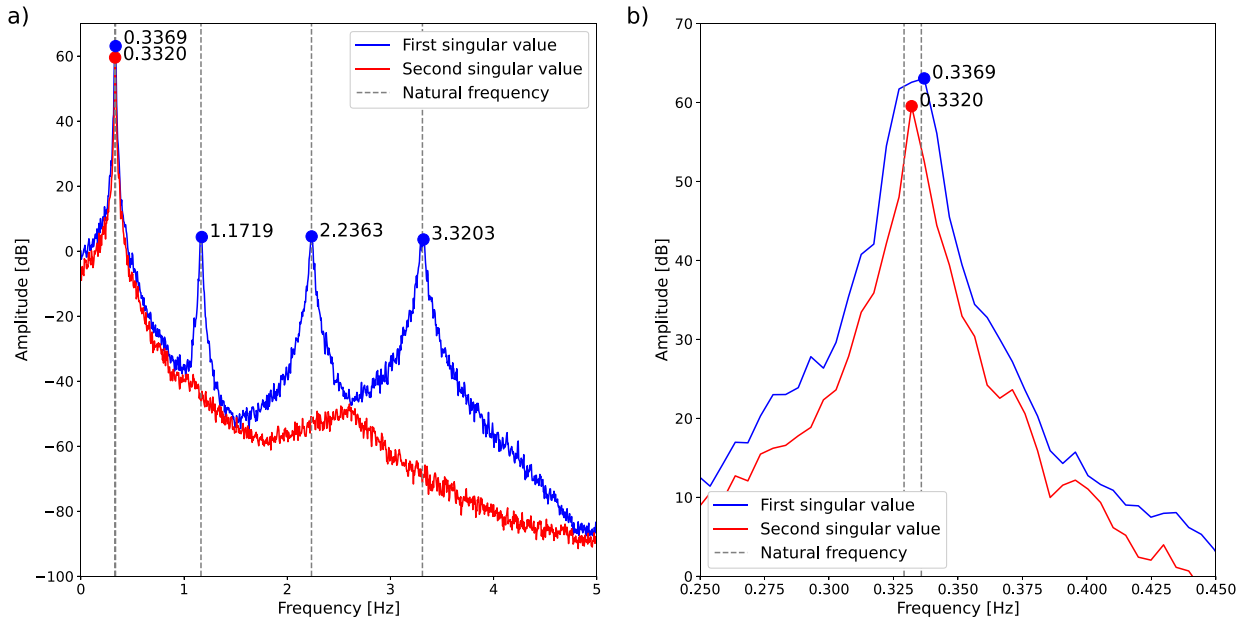

Fig. A.1. Modal identification using 2^{11} data points: (a) all identified modes; (b) close-up of closely spaced modes.

After this analysis, 2^{13} data points are suggested as segment length. Therefore, a 3-h dataset is generated to have 25 averages that overlap by 50%. Table A.2 and Fig. A.2 prove that the closely spaced modes can be identified correctly by using 2^{13} data points.

These results pose a problem because, on the one hand, a dataset of 3 h is not feasible for practical applications since the variability caused by environmental factors within a time frame of 3 h is likely to affect the OMA results [5]. On the other hand, shorter time series give biased mode shape estimations.

Loads with different magnitudes in the FA and the SS direction are applied to mitigate this problem. Rainieri and Fabbrocino [3] prescribe that the error of a biased mode shape estimation decreases if the difference between the first and the second singular values becomes larger. Hence, imposing the different magnitudes of the loads increases the difference between the first and the second singular value, and consequently, the error of the biased mode shape estimation decreases.

Table A.3 and Fig. A.3 show the modal identification results using 2^{11} data points and a 45-min dataset when the white noise excitation has a four times larger magnitude in the FA direction than in the SS direction. The results show that BM1-SS is estimated correctly when different magnitudes are used.

A different magnitude in the FA and the SS direction can be justified for an OWT since OWTs, in practice, are mainly loaded perpendicular to blades. Realistic loading behaviour still occurs for different magnitudes in both directions. Therefore, the difference in magnitude is applied to all load cases as prescribed in Section 3.3.

Table A.2
Modal identification using 2^{13} data points.

Mode	Natural frequency [Hz]		Error [%]	MAC [–]
	Modelled	Identified		
BM1 - SS	0.3291	0.3284	0.22	1.00
BM1 - FA	0.3358	0.3381	0.70	1.00
T	1.1641	1.1658	0.14	1.00
BM2 - SS	2.2350	2.2314	0.16	1.00
BM2 - FA	3.3100	3.3032	0.20	1.00

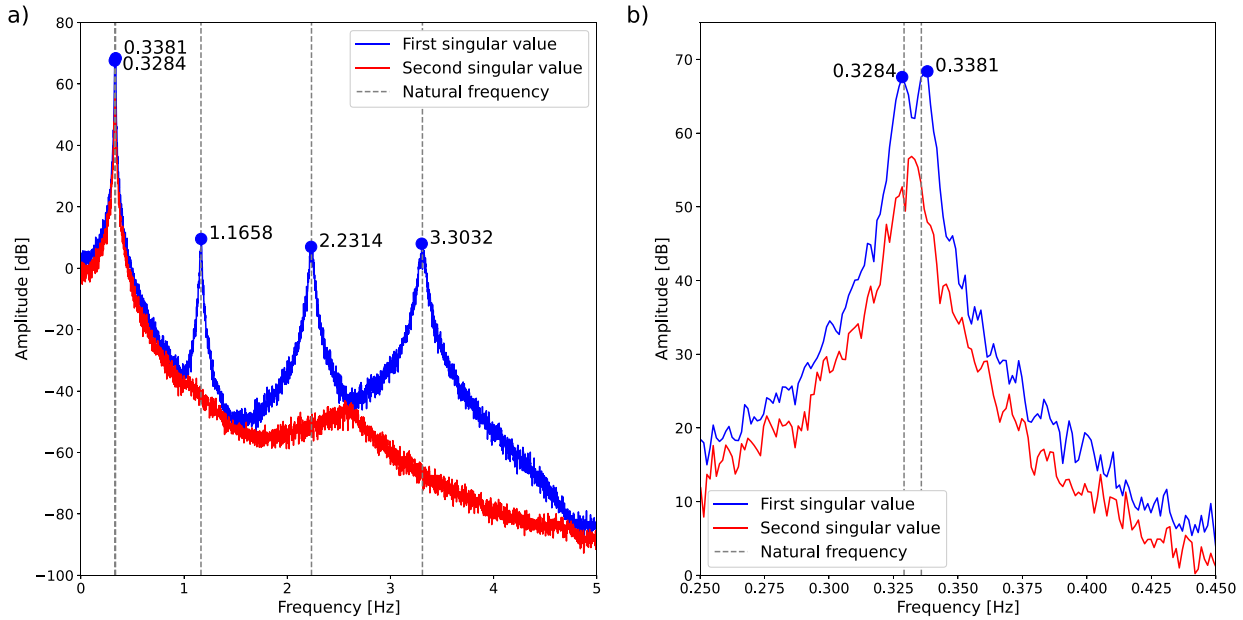

Fig. A.2. Modal identification using 2^{13} data points: (a) all identified modes; (b) close-up of closely spaced modes.

Table A.3
Modal identification using different magnitudes and 2^{11} data points.

Mode	Natural frequency [Hz]		Error [%]	MAC [–]
	Modelled	Identified		
BM1 - SS	0.3291	0.3320	0.89	1.00
BM1 - FA	0.3358	0.3369	0.33	1.00
T	1.1641	1.1670	0.25	1.00
BM2 - SS	2.2350	2.2266	0.38	1.00
BM2 - FA	3.3100	3.3105	0.02	1.00

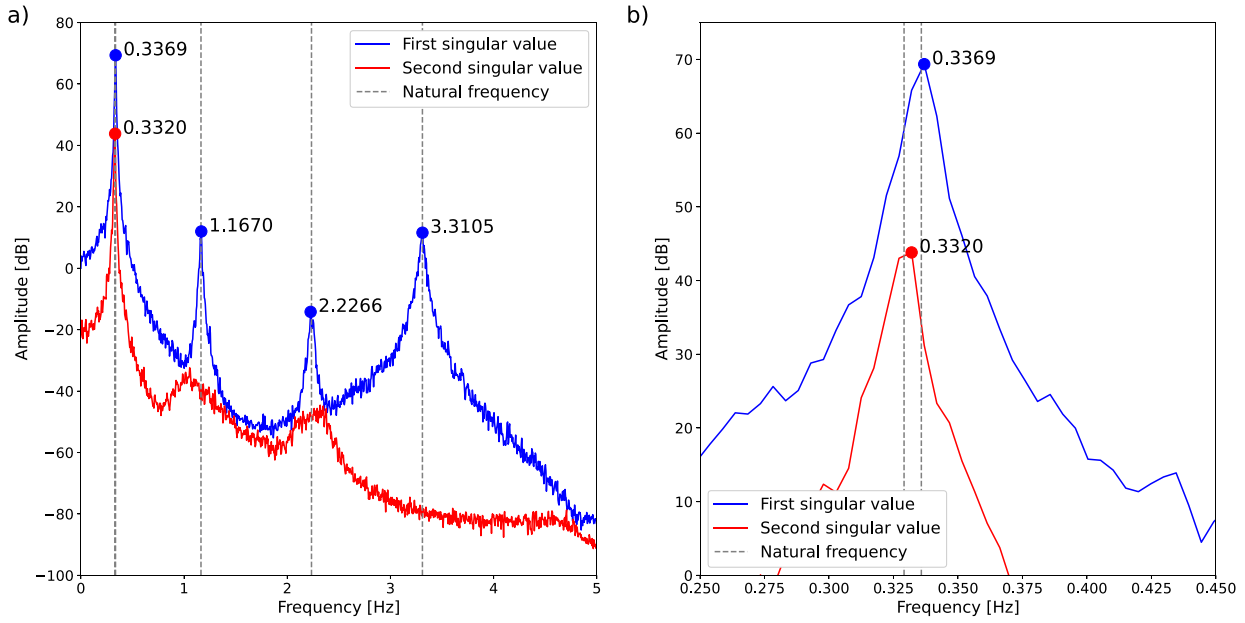

Fig. A.3. Modal identification using different magnitudes and 2^{11} data points: (a) all identified modes; (b) close-up of closely spaced modes.

References

[1] WES - Wind Energy Solutions, How many blades are best for wind energy production?, 2020, https://windenergysolutions.nl/uncategorized/how-many-blades, (accessed 2023).

[2] J.M.W. Brownjohn, Structural health monitoring of civil infrastructure, Philos. Trans. R. Soc. A Math. Phys. Eng. Sci. 365 (1851) (2007) 589–622, https://doi.org/10.1098/rsta.2006.1925.

[3] C. Rainieri, G. Fabbrocino, Operational Modal Analysis of Civil Engineering Structures, Springer New York, New York, NY, 2014, https://doi.org/10.1007/978-1-4939-0767-0.

[4] C. Devriendt, F. Magalhães, W. Weijtjens, G. De Sitter, Á. Cunha, P. Guillaume, Structural health monitoring of offshore wind turbines using automated operational modal analysis, Struct. Health Monit. 13 (6) (2014) 644–659, https://doi.org/10.1177/1475921714556568.

[5] W.-H. Hu, S. Thöns, R.G. Rohrmann, S. Said, W. Rücker, Vibration-based structural health monitoring of a wind turbine system Part II: environmental/operational effects on dynamic properties, Eng. Struct. 89 (2015) 273–290, https://doi.org/10.1016/j.engstruct.2014.12.035.

[6] G. Oliveira, F. Magalhães, Á. Cunha, E. Caetano, Modal decomposition of the dynamic response of wind turbine during one year of continuous monitoring, Struct. Control Health Monit. 28 (8) (2021) e2754, https://doi.org/10.1002/stc.2754.

[7] S. Pereira, J. Pacheco, F. Pimenta, C. Moutinho, Á. Cunha, F. Magalhães, Contributions for enhanced tracking of (onshore) wind turbines modal parameters, Eng. Struct. 274 (2023) 115120, https://doi.org/10.1016/j.engstruct.2022.115120.

[8] J.G. Kjeld, L.D. Avendaño-Valencia, J. Vestermark, Effect of wind and wave properties in modal parameter estimates of an idling offshore wind turbine from long-term monitoring data, Mech. Syst. Signal Process. 187 (2023) 109934, https://doi.org/10.1016/j.ymssp.2022.109934.

[9] E. Reynders, J. Houbrechts, G. De Roeck, Fully automated (operational) modal analysis, Mech. Syst. Signal Process. 29 (2012) 228–250, https://doi.org/10.1016/j.ymssp.2012.01.007.

[10] A. Cabboi, F. Magalhães, C. Gentile, Á. Cunha, Automated modal identification and tracking: application to an iron arch bridge, Struct. Control Health Monit. 24 (1) (2017) e1854, https://doi.org/10.1002/stc.1854.

[11] J. Zeng, Z. Hu, Automated operational modal analysis using variational Gaussian mixture model, Eng. Struct. 273 (2022) 115139, https://doi.org/10.1016/j.engstruct.2022.115139.

[12] E.M. Tronci, M. De Angelis, R. Betti, V. Altomare, Multi-stage semi-automated methodology for modal parameters estimation adopting parametric system identification algorithms, Mech. Syst. Signal Process. 165 (2022) 108317, https://doi.org/10.1016/j.ymssp.2021.108317.

[13] E. Tomassini, E. García-Macías, E. Reynders, F. Ubertini, Model-assisted clustering for automated operational modal analysis of partially continuous multi-span bridges, Mech. Syst. Signal Process. 200 (2023) 110587, https://doi.org/10.1016/j.ymssp.2023.110587.

[14] Q.-M. Zhong, S.-Z. Chen, Z. Sun, L.-C. Tian, Fully automatic operational modal analysis method based on statistical rule enhanced adaptive clustering method, Eng. Struct. 274 (2023) 115216, https://doi.org/10.1016/j.engstruct.2022.115216.

[15] M.D.H. Bhuyan, G. Gautier, N. Le Touz, M. Döhler, F. Hille, J. Dumoulin, L. Mevel, Vibration-based damage localization with load vectors under temperature changes, Struct. Control Health Monit. 26 (11) (2019) e2439, https://doi.org/10.1002/stc.2439.

[16] L.A. Bull, K. Worden, R. Fuentes, G. Manson, E.J. Cross, N. Dervilis, Outlier ensembles: A robust method for damage detection and unsupervised feature extraction from high-dimensional data, J. Sound Vib. 453 (2019) 126–150, https://doi.org/10.1016/j.jsv.2019.03.025.

[17] K. Tatsis, V. Dertimanis, Y. Ou, E. Chatzi, GP-ARX-based structural damage detection and localization under varying environmental conditions, J. Sens. Actuator Netw. 9 (3) (2020) 41, https://doi.org/10.3390/jsan9030041.

[18] W. Lin, K. Worden, A.E. Maguire, E.J. Cross, A mapping method for anomaly detection in a localized population of structures, Data-Centric Eng. 3 (2022) e25, https://doi.org/10.1017/dce.2022.25.

[19] L. Long, M. Döhler, S. Thöns, Determination of structural and damage detection system influencing parameters on the value of information, Struct. Health Monit. 21 (1) (2022) 19–36, https://doi.org/10.1177/1475921719900918.

[20] D. Tcherniak, S. Chauhan, M.H. Hansen, Applicability limits of operational modal analysis to operational wind turbines, in: T. Proulx (Ed.), Structural Dynamics and Renewable Energy, Volume 1, Conference Proceedings of the Society for Experimental Mechanics Series, Springer New York, New York, NY, 2011, pp. 317–327, http://dx.doi.org/10.1007/978-1-4419-9716-6_29.
[21] T.J. Larsen, T. Kim, Experimental and numerical study of rotor dynamics of a two- and three-bladed wind turbine, Int. J. Offshore Polar Eng. 26 (4) (2016) 355–361, https://doi.org/10.17736/ijope.2016.mmr12.
[22] M. Vergassola, A. Cabboi, P. van der Male, Comparative analysis of offshore support structures for two-bladed large wind turbines (10+MW) in deep waters, J. Phys. Conf. Ser. 1618 (5) (2020) 052076, https://doi.org/10.1088/1742-6596/1618/5/052076.
[23] C. Devriendt, P. Guillaume, The use of transmissibility measurements in output-only modal analysis, Mech. Syst. Signal Process. 21 (7) (2007) 2689–2696, https://doi.org/10.1016/j.ymssp.2007.02.008.
[24] W.J. Yan, M.Y. Zhao, Q. Sun, W.X. Ren, Transmissibility-based system identification for structural health monitoring: fundamentals, approaches, and applications, Mech. Syst. Signal Process. 117 (2019) 453–482, https://doi.org/10.1016/j.ymssp.2018.06.053.
[25] I.G. Araújo, J.A.G. Sánchez, P. Andersen, Modal parameter identification based on combining transmissibility functions and blind source separation techniques, Mech. Syst. Signal Process. 105 (2018) 276–293, https://doi.org/10.1016/j.ymssp.2017.12.016.
[26] V.D. Do, T.P. Le, A. Beakou, Operational modal analysis of mechanical systems using transmissibility functions in the presence of harmonics, J. Sci. Technol. Civ. Eng. (STCE) - NUCE 13 (3) (2019) 1–14, https://doi.org/10.31814/stce.nuce2019-13(3)-01.
[27] I.G. Araújo, J.E. Laier, R. Carrazedo, Enhanced power spectral density transmissibility matrix for operational modal analysis of structures, J. Struct. Eng. 145 (6) (2019) 04019043, https://doi.org/10.1061/(ASCE)ST.1943-541X.0002322.
[28] R. Brincker, L. Zhang, P. Andersen, Modal identification of output-only systems using frequency domain decomposition, Smart Mater. Struct. 10 (3) (2001) 441–445, https://doi.org/10.1088/0964-1726/10/3/303.
[29] W.J. Yan, W.X. Ren, Operational modal parameter identification from power spectrum density transmissibility, Comput.-Aided Civ. Infrastruct. Eng. 27 (3) (2012) 202–217, https://doi.org/10.1111/j.1467-8667.2011.00735.x.
[30] I.G. Araújo, J.E. Laier, Operational modal analysis using SVD of power spectral density transmissibility matrices, Mech. Syst. Signal Process. 46 (1) (2014) 129–145, https://doi.org/10.1016/j.ymssp.2014.01.001.
[31] A. Belouchrani, K. Abed-Meraim, J.-F. Cardoso, E. Moulines, A blind source separation technique using second-order statistics, IEEE Trans. Signal Process. 45 (2) (1997) 434–444, https://doi.org/10.1109/78.554307.
[32] J. Jonkman, S. Butterfield, W. Musial, G. Scott, Definition of a 5-MW Reference Wind Turbine for Offshore System Development, Technical Report NREL/TP-500-38060, National Renewable Energy Lab. (NREL), Golden, CO (United States), 2009.
[33] H. Panzer, J. Hubele, R. Eid, B. Lohmann, Generating a Parametric Finite Element Model of a 3D Cantilever Timoshenko Beam Using MATLAB, Technical Reports on Automatic Control Vol. TRAC-4, Institute of Automatic Control, Technische Universität München, 2009.
[34] M.S. Triantafyllou, G.S. Triantafyllou, Frequency coalescence and mode localization phenomena: a geometric theory, J. Sound Vib. 150 (3) (1991) 485–500, https://doi.org/10.1016/0022-460X(91)90899-U.
[35] E. Balmès, High modal density, curve veering, localization: a different perspective on the structural response, J. Sound Vib. 161 (2) (1993) 358–363, https://doi.org/10.1006/jsvi.1993.1078.
[36] R.J. Allemang, D.L. Brown, A correlation coefficient for modal vector analysis, in: Proc. of the 1st IMAC, 1982, pp. 110–116.
[37] E. Branlard, Wind Energy: Generation of Time Series from a Spectrum: Generation of Wind Times Series from the Kaimal Spectrum, Generation of Wave Times Series from the JONSWAP Spectrum, Tech. rep., Technical Univeristy of Denmark, 2010.
[38] Det Norske Veritas, Environmental Conditions and Environmental Loads, Recommended Practice DNV-RP-C205, Det Norske Veritas, 2010.
[39] J. Kang, H. Ju, L. Liu, Comparison of response transmissibility and power spectral density transmissibility on operational modal analysis, Mech. Syst. Signal Process. 160 (2021) 107912, https://doi.org/10.1016/j.ymssp.2021.107912.